ARKIV FÖR FYSIK Band 19 nr 39

Communicated 8 March 1961 by The Svedberg and Erik Rudberg

The elastic scattering of 180 MeV protons from nuclei

By A. Johansson, U. Svanberg and P. E. Hodgson

With 35 figures in the text

ABSTRACT

The differential cross sections for elastic scattering of 180 MeV protons from lithium, beryllium, carbon, aluminium, calcium, iron, indium and gold have been measured up to large scattering angles. Particular care was taken to obtain good energy resolution. The results have been compared with the calculated scattering from an optical model potential with different radial extensions of the real and imaginary terms in both the central and the spin-orbit parts of the potential. Qualitative agreement was found.

1. Introduction

The differential cross sections for elastic scattering of high energy protons from nuclei have been measured in many experiments ever since the first beams of such protons were available from accelerators. On most occasions, however, the measurements have been confined to small angles and in some cases the energy resolution has been insufficient to make sure that the cross sections determined were unaffected by inelastic scattering.

Many analyses of high energy proton scattering data have been made using optical model potentials. Several reviews have been written [1, 2, 3], where references are given both to theoretical and experimental work. Usually the real and the imaginary central terms of the potential have been assumed to have the same radial dependence and the spin-orbit terms to be proportional to the gradient of the central parts. However, such a potential is insufficient to explain the scattering from comparatively light nuclei [4, 5, 6]. A more general potential with different form factors greatly increases the number of adjustable parameters in a phenomenological fitting procedure and consequently requires more experimental results for a successful analysis; large angle data should be particularly useful.

Under certain assumptions it has been possible to reduce the actual many-body problem of the scattering of a high energy proton from a complex nucleus to the problem of the scattering of a proton from a generalized two-body potential, which however is non-local for finite nuclei (see for instance [7]). In a local approximation the optical model potential is obtained from the nucleon-nucleon scattering matrix and the nuclear density. If the angular dependence of this matrix is taken into account the form factors of the potential will differ from each other. Unfortunately, the validity of the local approximation is questionable for scattering angles larger than the first diffraction minimum.

The first part of this paper reports on measurements of the differential cross sections for elastic scattering of 180 MeV protons from eight nuclei from lithium to gold with good energy resolution, the effort being concentrated on large angles. As measurements at small angles where the inelastic scattering is negligible would rather require a good angular than energy resolution and thus a quite different experimental arrangement, only very few small-angle cross sections were determined.

The second part of the paper consists of an optical model analysis of the differential cross sections together with reaction cross sections reported in the accompanying paper [8] and previously published polarizations [6, 9–13]. Two types of fits have been tried, one purely phenomenological and the other using the Gammel-Thaler nucleon-nucleon potential and nuclear densities derived from electron scattering data [14].

2. Experimental

2.1. *General considerations*

The main experimental problem in determining the differential cross sections for elastic scattering from nuclei at large angles is to obtain sufficiently good energy resolution. In the present experiment essentially the same method was used as that

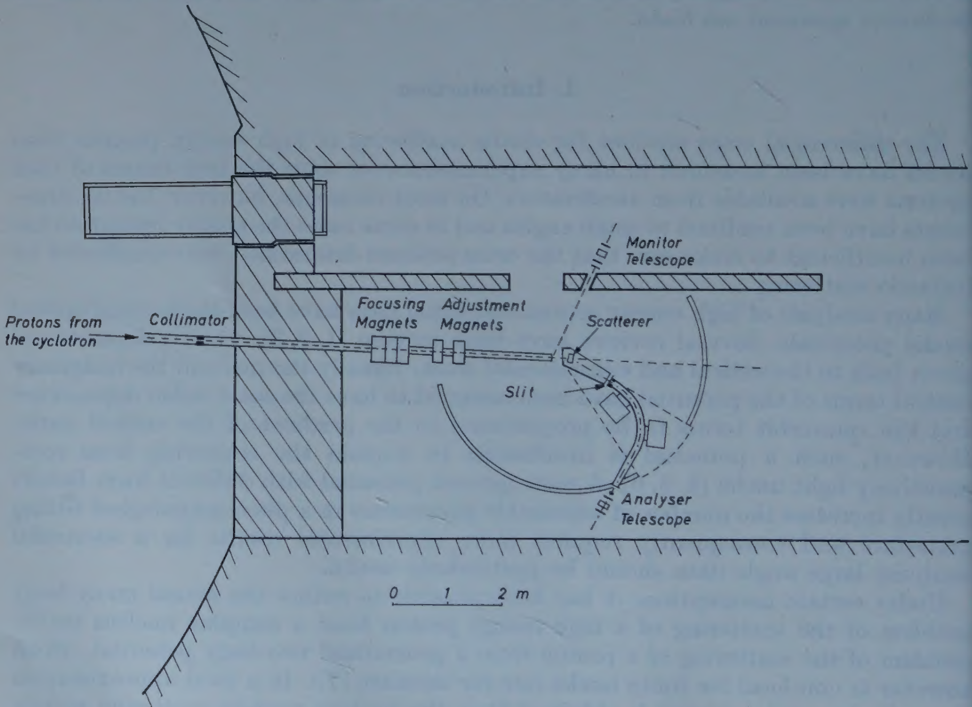

Fig. 1. Plan view of the experimental arrangements.

adopted by Tyrén and Maris [15] to measure differential cross sections for inelastic scattering; i.e. the separation of elastically and inelastically scattered protons was acquired by using a magnetic spectrometer which could be rotated about the scatterer. The experimental lay-out is shown in Fig. 1.

The incoming beam was the external, unpolarized beam of 187 MeV protons from the Uppsala synchrocyclotron. The energy spread was not known but was definitely less than 1 MeV full width at half height.

The protons that emerged from the spectrometer were detected by a counter telescope of three scintillation counters in coincidence, the width of the defining crystal being so small that it did not appreciably reduce the resolution. The incident beam was monitored by another telescope looking at the end window of the proton tube.

The area under a spectrum peak corresponding to elastically scattered protons is proportional to the elastic differential cross section. The proportionality factor is very nearly independent of the peak width if the momentum or the energy of the protons is taken as abscissa, but it is still a function of the magnetic field and the proton energy. The determination of this factor is considered in section 2.5. and was based on values from other experiments for the free p–p scattering cross section.

2.2. *The magnetic spectrometer*

The main properties of the magnetic spectrometer have been described by Tyrén and Maris [15]. Some changes of its field shape were made, however, to improve the accuracy of the instrument.

The magnetic field was not quite homogeneous in the whole region where protons passed due to the small width of the pole tips. (The gap was 75 mm wide and 16 mm high.) This would probably reduce the energy resolution and, what would be more serious, make the transmission of the protons dependent on the proton path inside the spectrometer. It was not practical to use such a small height of the entrance slit that all protons were prevented from hitting the pole faces and defocusing (and focusing) forces due to magnetic field gradients would thus strongly affect the transmission. Therefore, the field shape was altered at two places along the proton path by shimming in such a way that the direction of the gradients were reversed. The effect of these shims was then to make every proton pass through successive regions of vertically focusing and vertically defocusing forces, the net effect of which was approximately zero. The energy resolution should also be improved by this shimming because the average value of the magnetic field experienced by a proton was made nearly independent of the path.

The second change consisted of a careful shaping of the fringing field both at the entrance and at the exit to make it satisfy the theoretical requirements more rigorously.

As a result of these changes the following improvements were found experimentally:

(1) The transmission of protons entering at different points of the opening slit, which was 8 mm high and 12 mm wide, was constant within a statistical uncertainty of a few per cent.

(2) Within 5 % the transmission of protons was found to be independent of changes in the beam position at the scatterer of ± 1.5 mm vertically and ± 10 mm horizontally. This was quite sufficient to make sure that the errors that could arise from small beam displacements or from the use of thick targets at large scattering angles were negligible.

(3) The total width at half height of a peak of scattered protons from a thin target was only 1.00 MeV, a figure which includes both the energy spread of the incoming beam and the resolution of the spectrometer. It was not possible to determine the relative contribution from the two sources. Before the field modifications the half width was 1.6 MeV.

It was found that the extensive fringing field gave rise to a shift in the beam position at the scatterer, a shift that varied not only with the magnetic field but also with the angular position of the spectrometer. By small adjustment magnets (see Fig. 1) about two meters in front of the scatterer the beam was always brought to the same position, and corrections were applied to the zero degree correction angle.

Immediately before and after the measurement of a peak, the beam position at the scatterer was determined by exposing a photographic paper. It was thus ensured that no changes had occurred either in the vertical direction, which might have altered the transmission, or in the horizontal direction which would have deformed the peak shape.

In a scattering experiment the scatterer is usually set at such an angle that the normal to the target surface bisects the scattering angle. All protons then have equal path lengths in the target and they emerge with approximately the same energy. In this experiment the target angle was chosen more elaborately to obtain as small peak widths as possible. The following sources of energy spread were considered and eliminated to first order by a proper choice of target angle: (*a*) the differences between the recoil energy loss in the beginning and the end of the target, (*b*) the nonlinear variation of ionization energy loss with proton energy, and (*c*) the width of the beam as seen from the spectrometer.

2.3. *Electronics*

Due to the fact that the duty cycle of the external beam from the cyclotron was very small (about 1/400) there was a risk of counting losses even at moderate counting rates. Moreover, the duty cycle was not very constant in time which would have made corrections for the counting losses due to dead time very uncertain, so that fast counting systems were needed.

Two scale-of-four units were built with fast transistors (2N 501) and used in the monitor and the spectrometer detecting systems. The resolving time for two consecutive pulses was 25 nsec and consequently two protons appearing in two consecutive r.f. bursts of the proton beam could be resolved. The pulses from the fast scalers were fed into conventional 1 Mc scalers.

The systems of photomultipliers, coincidence units and scalers were tested with varying counting rates, and counting losses were found to be less than 1 % for counting rates up to 10^3 protons/sec average rate. The number of protons detected per second was always in the experiment kept less than 10^3, so that errors due to dead time losses should be negligible.

2.4. *Energy calibration*

A calibration curve for transformation from spectrometer current to proton energy was obtained by measuring the current at the maxima of a series of peaks from *p*–*p* scattering at several angles and from elastic and inelastic scattering from carbon. However, as the half-width of a peak was about 1.00 MeV an accuracy of 1 %, for instance, in the area determination required a precision in the current readings corresponding to about 0.01 MeV. Although the operation of the spectrometer always was in the region of strongly saturated iron, the ordinary current instrument could not provide this accuracy. For this purpose a device was used which consisted of two anticoupled coils in series with each other and with a sensitive fluxmeter. The coils were placed in the fringing field of the spectrometer and one of them between two mumetal bars. Each coil was shunted by an external resistance and the actual reading consisted of an adjustment of one of the shunt resistances to give zero deflection on the galvanometer when the two coils were flipped simultaneously. By a suitable choice of coil sizes the device was made extremely sensitive to changes in the magnetic field in the range necessary for the experiment. The resistance readings were put on an absolute scale each time a peak was measured by comparing with current readings and using the calibration curve mentioned above. Thus the errors from the uncertainty in the energy setting of the spectrometer is small in most measurements.

2.5. *Transmission and efficiency calibrations*

To be able to convert the area under a spectrum peak into an absolute value for the differential cross section one should know the following parameters:

(*a*) The transmission of protons by the spectrometer magnet.

(*b*) The effective solid angle for the scattering. The fringing field of the magnet extended outside the entrance slit and consequently the effective solid angle was dependent on the focusing properties of the field.

(*c*) The detection efficiency of the spectrometer counter telescope. Between the second and the third counter of this telescope was inserted a copper absorber to prevent particles of low energy from being detected. Such particles could be protons having passed through the spectrometer by scattering on collimator edges or pick-up deuterons of the correct momentum to pass freely through the magnet. The efficiency was thus less than one mostly due to losses of elastic protons in this copper absorber.

(*d*) The equivalent width in proton energy (= the abscissa of the spectra) of the defining crystal of the telescope.

(*e*) The conversion factor between monitor counts and number of protons hitting the target.

The first four of these parameters are dependent on the magnetic field, i.e. on the energy of the elastically scattered protons.

Each of these five parameters was not measured separately. By determining the area under the peak for free proton-proton scattering from polythene minus carbon at some angles and using the relatively well known results for the p–p differential cross section, a calibration curve could be constructed for the product of all the five parameters versus proton energy. One additional advantage of this method was that any error in the energy calibration curve was eliminated from the end results. The reduction in beam intensity due to inelastic collisions in the target were corrected for. The values for the p–p cross section, which were used, are given in Table 1 and were obtained by an interpolation between published data [16–19].

Since the main absolute error of the cross sections reported in this paper originates in the uncertainty of the p–p cross sections, a future improvement of the latter would also improve on the results given in Tables 2–9.

Table 1. The values used for the p–p differential cross section at 180 MeV laboratory energy.

Lab. angle (degrees)	CM angle (degrees)	CM cross section (mb/sterad)	Lab. cross section (mb/sterad)
8.5	17.8	3.74	16.16
10.0	20.9	3.73	16.02
11.8	24.7	3.75	15.98
13.3	27.8	3.76	15.89
14.3	29.9	3.76	15.80
17.0	35.5	3.75	15.48
19.4	40.5	3.72	15.07
21.7	45.3	3.68	14.61
23.7	49.4	3.64	14.18
25.5	53.1	3.61	13.80
27.1	56.4	3.57	13.40

The long time constancy of the calibration curve was checked by frequent remeasurements of a few carbon cross sections. Except on one occasion when a short circuit had occurred in the spectrometer no significant changes were found.

2.6. *The angular resolution*

As the elastic differential cross section varies extremely rapidly with angle nearly everywhere, it is of great interest to know the angular resolution function of the scattering, i.e. the resolution including the angular spread of the incoming beam, the beam width at the scatterer, the width of the entrance opening, and the multiple scattering in the scatterer. Therefore, the spectrometer telescope was replaced by an ionization chamber sufficiently large to cover the whole emerging beam. The spectrometer was swept through the zero degree position with a few different targets at the usual scattering centre. In this manner were obtained not only the shape of the resolution function and its dependence on the multiple Coulomb scattering in the targets, but also the true spectrometer zero degree position which differed about 0.7° from the nominal setting due to the extensive fringing field of the magnet.

The experimental points for the resolution function were found to lie on a Gaussian with a total width at half height of 0.8° when the effects of multiple scattering were subtracted. The angular resolutions (with multiple scattering effects included) are given in Tables 2–9.

There was a finite possibility for protons to be scattered twice in the target through wide scattering angles. The angular distribution of this double scattering would be expected to follow that for single scattering except for the absence of sharp diffraction patterns. The effect would thus be most serious at the diffraction minima. An estimate was made which showed that double scattering could have contributed at most a few per cent to the elastic cross section obtained with the thickest targets used.

2.7. *Determination of peak areas*

A method was developed which permitted a convenient evaluation of the area under a peak known at some discrete points from experiment and also made it pos-

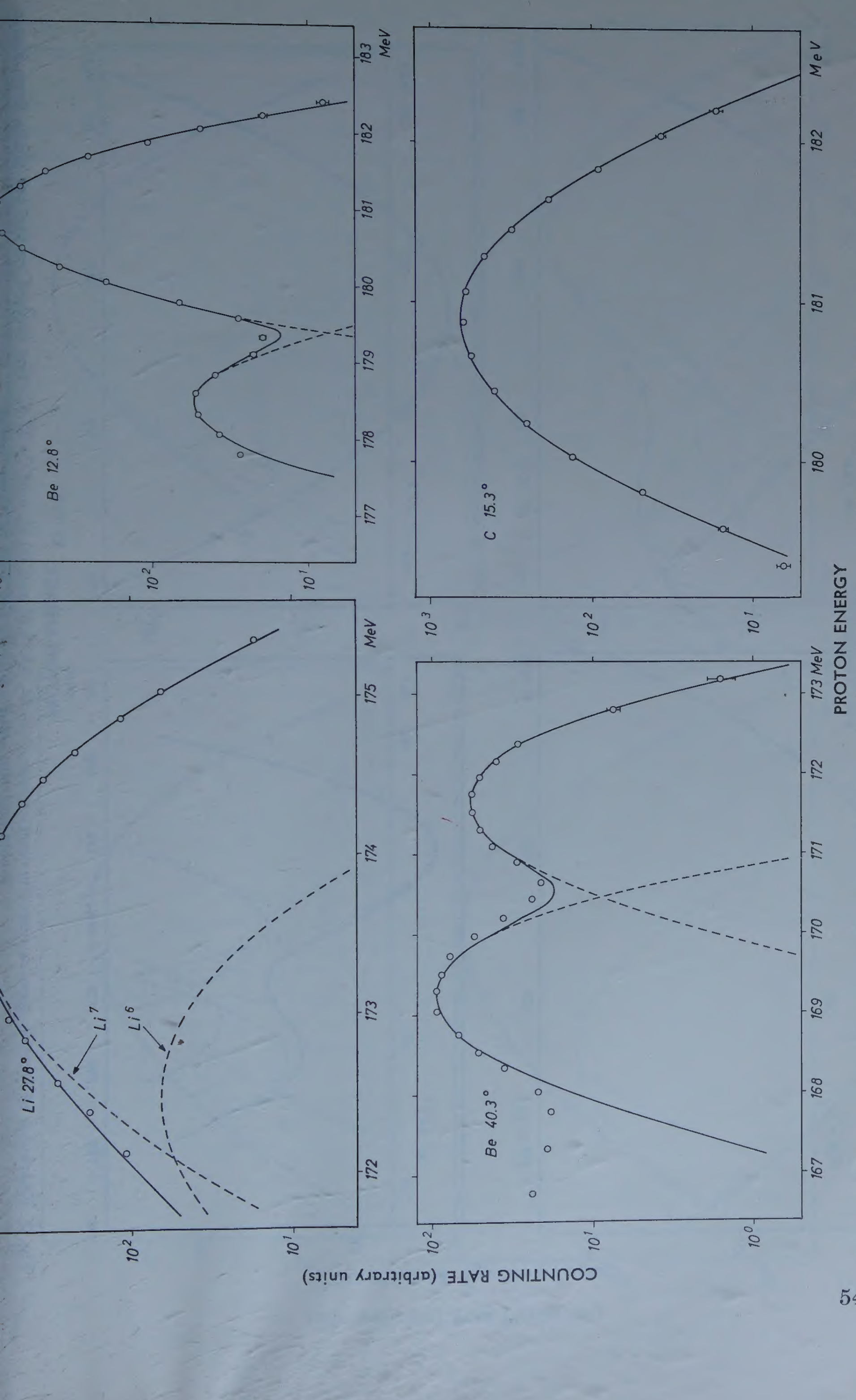

Fig. 2. Examples of proton spectra near the elastic peak: Li 27.8°, Be 12.8° and 40.3°, and C 15.3°. The dashed curves are peaks from single levels and the solid curve is the sum of these peaks.

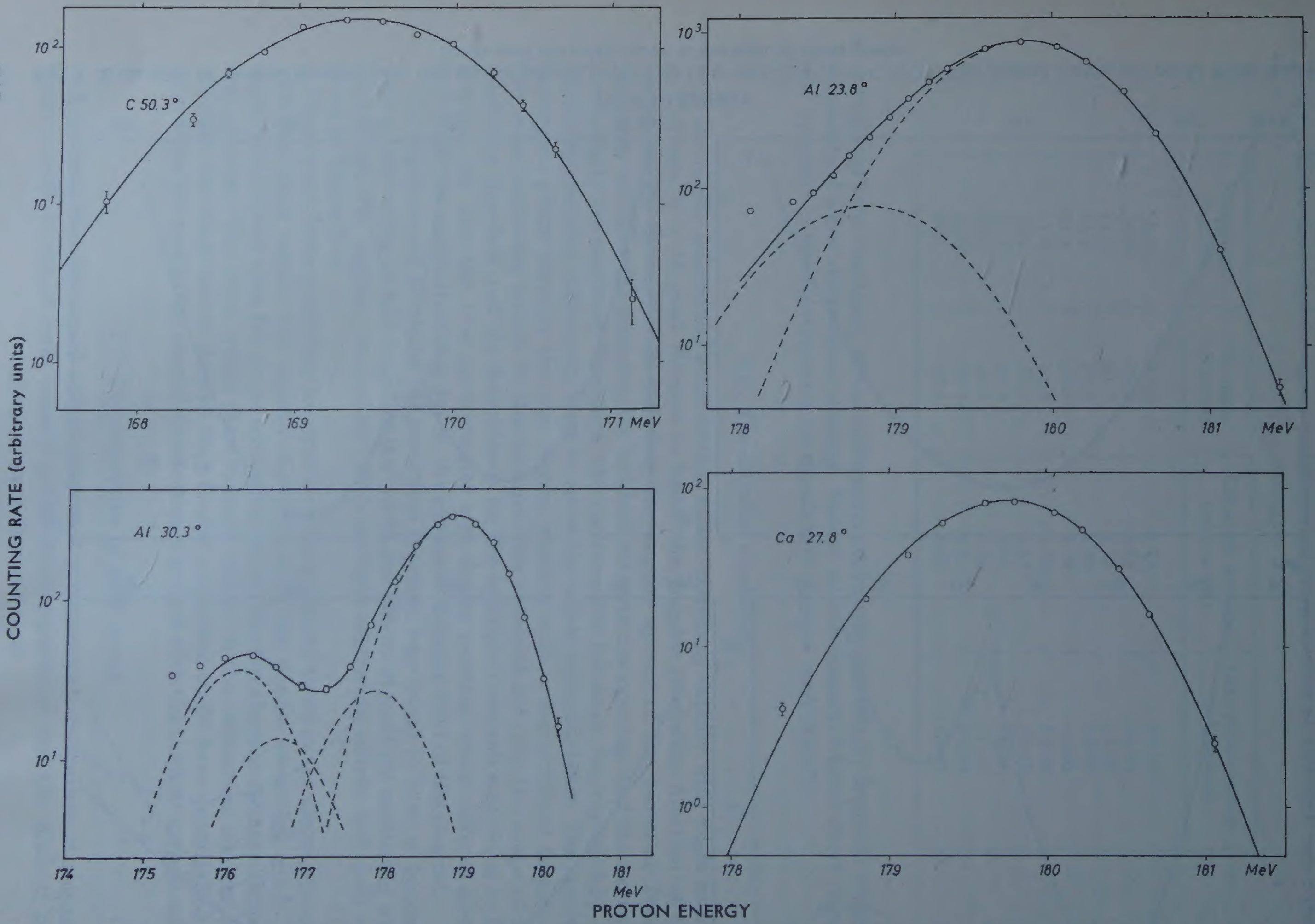

Fig. 3. Examples of proton spectra near the elastic peak: C 50.3°, Al 23.8° and 30.3°, and Ca 27.8°. The dashed curves are peaks from single levels and the solid curve is the sum of these peaks.

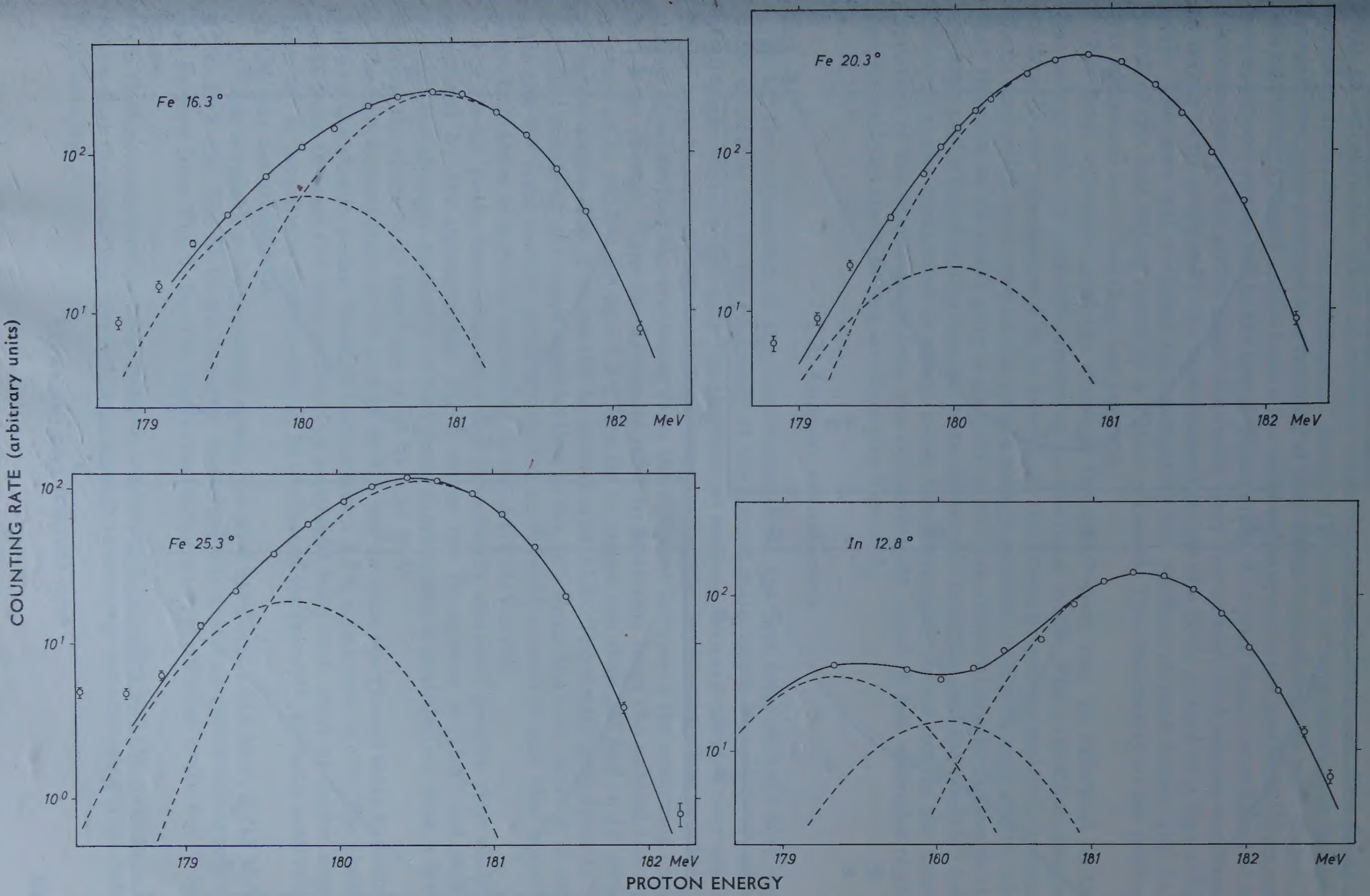

Fig. 4. Examples of proton spectra near the elastic peak: Fe 16.3°, 20.3° and 25.3°, and In 12.8°. The dashed curves are peaks from single levels and the solid curve is the sum of these peaks.

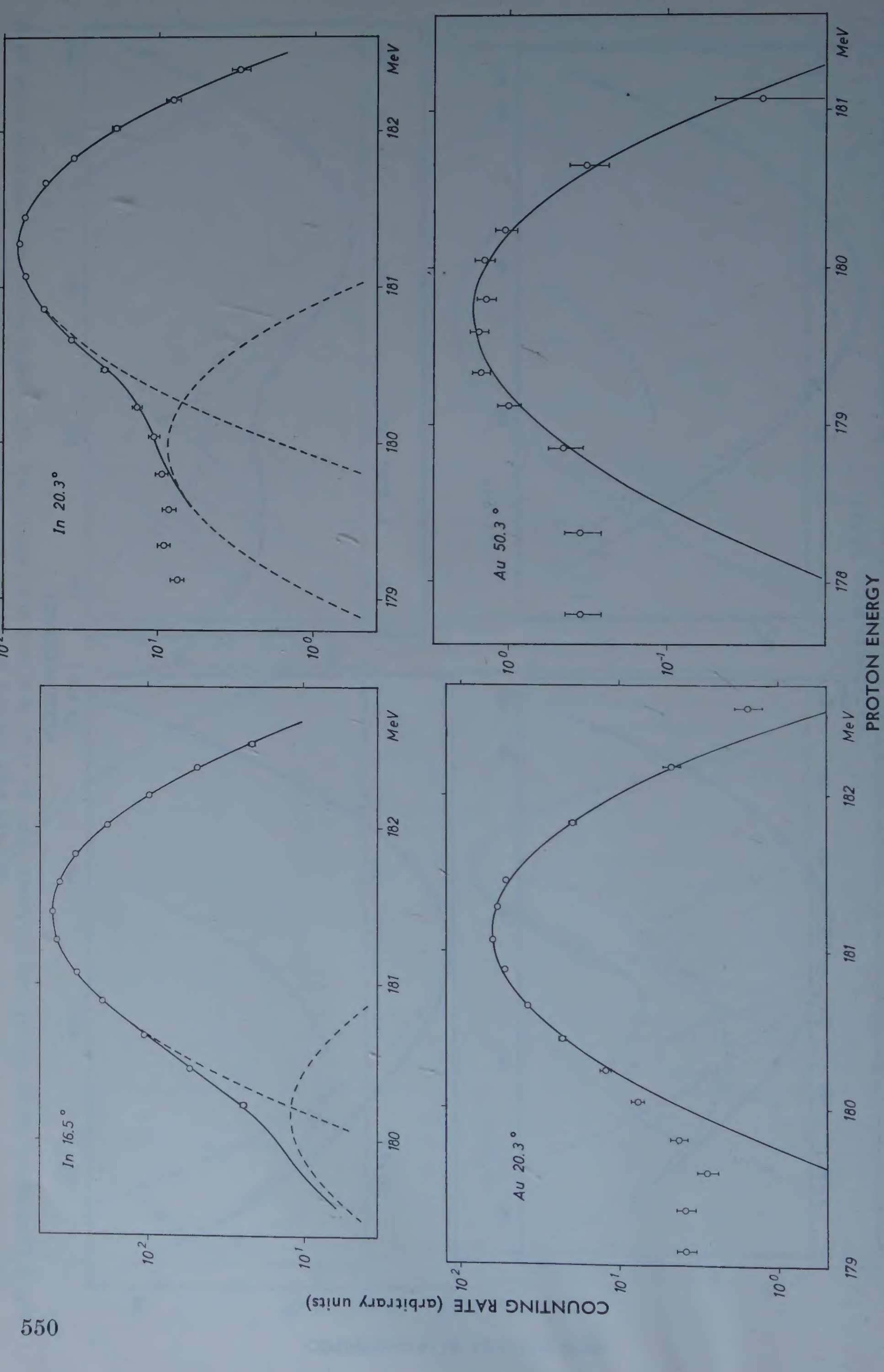

Fig. 5. Examples of proton spectra near the elastic peak: In 16.5° and 20.3°, Au 20.3° and 50.3°. The dashed curves are the peaks from single levels and the solid curve is the sum of these peaks

sible to estimate the effect of inelastic scattering to low-lying levels. The *forms* of spectrum peaks from "monoenergetic" groups of protons, i.e. protons without inelastic admixtures, were deduced as a function of half width by studying the peak shapes in the scattering at small angles from a few different targets, in the scattering from carbon at several angles and in the free p–p scattering. The peak shapes were found to be Gaussian except for a very slight skewness. Only curves with such shapes were used in trying to fit graphically the experimental points of a peak plotted on a logaritmic scale. The area was obtained by multiplying the product of peak height and half width of the best-fitting curve by a known constant. The uncertainty in the method was estimated to be less than one per cent.

For most scatterers used the shape of the elastic peak may be deformed on the low-energy side by inelastic scattering to low-lying levels. The excitation energies of these levels were assumed to be known. In the fitting procedure peaks of the same shape and width were used at the proper energy positions and with such magnitudes that the sum of all peaks gave a good fit to the experimental points. Although the inelastic peaks found in this manner were often very uncertain and the resolving into different peaks ambiguous in many cases, the uncertainty introduced in the determination of the elastic peak area was comparatively small. A few examples of the spectra and the curve fitting are shown in Figs. 2–5.

2.8. *Inelastic contributions*

In Li^7 the subtraction of the contribution from the first level at 0.478 MeV was quite uncertain due to the proximity of the ground state, but it was relatively small at all angles and consequently the elastic cross sections were not affected very much. As all targets were of natural isotopic composition the recoil energy loss provided a means of separating the scattering from the different isotopes if the scattering angle was large enough. Thus the Li-results refer to scattering from the natural isotopic mixture of Li (92.5 % Li^7 and 7.5 % Li^6) up to angles less than 25° and to Li^7 alone for larger angles. Fig. 2 shows the Li spectrum at 27.8°. The elastic peak from Li^6 is included assuming the same cross section as for Li^7. From the sum curve it is seen that the Li^6 cross section probably should be reduced somewhat and that there is some indication of inelastic scattering to the 0.478 MeV level.

For Be the peaks from elastically and inelastically scattered protons were clearly separated by the spectrometer. Fig. 2 shows the Be spectra at 12.8° and 40.3°. Besides the strongly excited 2.43 MeV level there is also a contribution from a level or from the three-body break-up of Be at 1.75 MeV.

The first excited state in C^{12} at 4.43 MeV is too far from the ground state to contribute to the elastic peaks. Natural carbon has a 1.1 % admixture of C^{13}. The elastic peaks from C^{12} and C^{13} were sufficiently separated from each other at angles larger than 55° to permit the cross section to be evaluated for pure C^{12}. Inelastic scattering in C^{13} was not considered.

Al^{27} has several low-lying excited states, viz. at 0.842 MeV, 1.013 MeV, 2.213 MeV, 2.732 MeV etc. The fit to the inelastic scattering was therefore rather ambiguous as can be seen from Fig. 3, but the elastic scattering was nevertheless quite well determined.

In Ca^{40} no contribution from inelastic scattering is expected and the nucleus is so heavy that the recoil loss was not large enough to separate the scattering from different isotopes.

The first two excited states of Fe^{56} occur at 0.845 MeV and 2.085 MeV. The inelastic scattering to the 0.845 MeV level seems to be fairly large. Fig. 4 shows the angular variation of the peak shapes due to inelastic scattering as the elastic cross section passes through a maximum.

In^{115} and Au^{197} have many levels within the experimental resolution, and the evaluation of the elastic cross sections is correspondingly uncertain. As the elastic peak is dominant at all angles the cross sections in Tables 2–9 are believed to be reasonably free from inelastic contamination. Figs. 4 and 5 show a few examples of the spectra from these nuclei.

3. Results

In Tables 2–9 are given the differential cross sections, the scattering angles, the rms angular resolution and the mean proton energy, all in the laboratory system. The quoted errors in the cross sections are combined from the following sources:

(1) Counting statistics.

(2) Relative errors in the graphical method of determining areas.

(3) Relative errors in the calibration curve.

(4) Errors due to the subtraction of inelastically scattered protons.

(5) Uncertainty of the relative spectrometer field measurement. Relative errors due to an incorrect angular dependence of the *p–p* differential cross sections of Table 1 were not considered.

In addition there is an uncertainty of the scattering angle of ± 0.05° due to variations in the incoming beam direction and difficulty of positioning the spectrometer at the correct angle.

The absolute errors are caused by the uncertainty of the *p–p* cross section data given in Table 1, and should be less than about 10 %.

Table 2. Lithium.

Scattering angle θ_{lab} (degrees)	Rms angular resolution $\Delta\,\theta_{lab}$ (degrees)	Differential cross section σ_{lab} (mb/sterad)		Mean proton energy E_{lab} (MeV)
5.34	0.52	191.6	± 6.4	181.9
7.84		204.7	3.2	
10.34		146.6	2.7	
12.82		93.3	2.3	
15.32		55.4	1.1	
17.80		31.27	0.57	
20.32		17.02	0.37	
25.32	0.46	5.866	0.097	182.8
27.82		3.455	0.069	
30.31		2.283	0.041	
32.83		1.623	0.031	
35.31		1.099	0.029	
37.81		0.730	0.038	
40.31		0.482	0.012	
45.30		0.2069	0.0056	
50.31		0.0728	0.0031	
55.31		0.0303	0.0020	
60.31		0.0108	0.0011	
65.31		0.00587	± 0.00073	

Table 3. Beryllium.

Scattering angle θ_{lab} (degrees)	Rms angular resolution $\Delta\,\theta_{\text{lab}}$ (degrees)	Differential cross section σ_{lab} (mb/sterad)		Mean proton energy E_{lab} (MeV)
7.82	0.50	271.4	±4.1	182.7
10.31		196.7	2.9	
12.80		121.0	1.9	
15.32		64.93	0.99	
17.81		30.57	0.51	
20.31		14.74	0.20	
22.82		7.05	0.10	
25.31		3.846	0.068	
27.85		2.334	0.045	
30.31		1.567	0.034	
32.81		1.050	0.022	
35.32		0.734	0.017	
40.31		0.3225	0.0064	
45.31		0.1291	0.0040	
50.31		0.0467	0.0019	
55.31		0.01571	0.00054	
60.31		0.00470	0.00041	
60.31	0.51	0.00519	0.00040	181.5
65.31		0.00276	0.00030	
70.31		0.00105	±0.00016	

4. Optical model analysis

4.1. *General*

A two-body local optical model interaction of the form

$$V(r) = V_{\text{Coul}}(r) + U f_1(r) + i\,W[\alpha f_2(r) + (1-\alpha)\,g(r)] + \left(\frac{\hbar}{m_\pi c}\right)^2 \cdot \left[U_S \frac{d f_3(r)}{d r} + i\,W_S \frac{d f_4(r)}{d r}\right] \cdot \frac{1}{r}\,\boldsymbol{l}\cdot\boldsymbol{\sigma} \qquad (1)$$

was used where the form factors are given by

$$f_i(r) = \frac{1}{1+\exp\left(\dfrac{r-R_i}{a_i}\right)},$$

$$g(r) = \exp\left[-\left(\frac{r-R_2'}{b}\right)^2\right]. \quad \text{and} \quad R_i = r_i N^{1/3}.$$

N denotes the number of nucleons in the target nucleus. $V_{\text{Coul}}(r)$ is the Coulomb potential from a uniformly charged sphere of radius $1.3 \cdot N^{1/3} \cdot 10^{-13}$ cm, U and W are the real and imaginary parts of the central potential and U_S and W_S the corresponding spin-orbit potentials. The imaginary or absorbing part of the central potential has

Table 4. Carbon.

Scattering angle θ_{lab} (degrees)	Rms angular resolution $\Delta\,\theta_{\mathrm{lab}}$ (degrees)	Differential cross section σ_{lab} (mb/sterad)		Mean proton energy E_{lab} (MeV)
6.31	0.52	371.7	±6.3	182.8
8.32		350.4	6.0	
10.30		280.4	3.7	
12.82		169.2	3.0	
15.30		98.0	1.2	
16.78		64.5	1.0	
17.80		47.03	0.62	
19.67		26.52	0.45	
20.30		22.37	0.34	
22.79		10.44	0.17	
23.98		7.36	0.15	
24.31		6.40	0.12	
25.27		5.235	0.097	
26.52		3.683	0.088	
27.39		3.023	0.050	
27.81		2.609	0.083	
28.33		2.204	0.035	
30.27		1.459	0.044	
32.32		0.902	0.018	
32.81		0.835	0.030	
35.29		0.5462	0.0077	
37.31		0.4506	0.0072	
37.80		0.433	0.016	
39.23		0.3701	0.0056	
40.27		0.349	0.012	
42.78		0.283	0.012	
43.31		0.2879	0.0058	
45.28		0.2472	0.0036	
46.50		0.2056	0.0049	
47.31		0.1885	0.0041	
47.76		0.1797	0.0090	
48.52		0.1639	0.0046	
50.28		0.1091	0.0024	
51.50		0.0961	0.0032	
52.80		0.0718	0.0038	
55.26		0.0440	0.0026	
55.26	0.72	0.0437	0.0017	177.1
60.27		0.01448	0.00064	
65.27		0.00513	0.00027	
70.27		0.00285	0.00024	
75.27		0.00183	0.00019	
80.28		0.00104	±0.00011	

a form factor that is an arbitrary mixture of Saxon-Woods and Gaussian forms, controlled by a mixing parameter α. The other symbols have their usual meanings. If this potential is inserted in the appropriate Schrödinger wave equation the corresponding observables can be calculated by the methods described elsewhere [20]. Except for a few preliminary runs all the calculations in the present work were done on the Oxford Mercury electronic computer.

Table 5. Aluminium.

Scattering angle θ_{lab} (degrees)	Rms angular resolution $\Delta\,\theta_{\text{lab}}$ (degrees)	Differential cross section σ_{lab} (mb/sterad)		Mean proton energy E_{lab} (MeV)
7.81	0.55	977.2	±19.5	183.0
10.31		575.6	9.8	
12.81		257.3	4.4	
15.30		94.18	1.42	
17.80		30.29	0.39	
19.81		16.15	0.22	
20.27		13.27	0.46	
21.31		11.82	0.23	
21.52		11.61	0.20	
22.76		9.69	0.24	
23.30		10.54	0.21	
23.76		10.09	0.11	
24.02		10.02	0.18	
25.27		8.72	0.13	
26.54		7.515	0.098	
27.79		5.921	0.089	
30.26		3.944	0.055	
32.77		2.302	0.046	
35.25		1.402	0.051	
36.32		1.083	0.021	
37.77		0.818	0.017	
40.23		0.418	0.013	
42.75		0.2286	0.0066	
45.29		0.1310	0.0030	
47.76		0.0881	0.0026	
50.25		0,0626	0.0018	
50.27	0.91	0.0726	0.0023	177.7
55.31		0.0232	0.0019	
60.29		0.00886	0.00054	
65.27		0.00337	0.00056	
70.27		0.00158±	0.00022	

4.2. *Phenomenological approach*

The general form of the potential (1) contains 15 adjustable parameters whereas the most commonly used optical potential with all f_i's identical and $\alpha = 1$ has only six. Although the present data on differential cross sections out to high angles, together with existing polarization measurements [6, 9–13] and reaction cross sections [8], provide more complete sets of experimental data than have hitherto been available they would probably not be sufficient for unique values of all 15 parameters to be determined in a free search. Therefore, in the phenomenological analysis described below, essentially seven parameters were varied, viz. U, W, U_S, W_S, $r_1 = r_3$, $r_2 = r_4$, $a = a_1 = a_2 = a_3 = a_4$. A few trials were made with $\alpha \neq 1$, but otherwise the absorbing part was always kept in the Saxon-Woods form.

In previous optical model analyses of proton scattering at high energies using six parameters quantitative fits were obtained to the small-angle data [4, 6, 21–23]. If the same parameters are used to calculate the differential cross sections corresponding to the present data it is found that in all cases they show marked oscillations, whereas

Table 6. Calcium.

Scattering angle θ_{lab} (degrees)	Rms angular resolution $\Delta\,\theta_{\text{lab}}$ (degrees)	Differential cross section σ_{lab} (mb/sterad)		Mean proton energy E_{lab} (MeV)
5.32	0.62	3120	±110	181.5
7.81		1815	49	
10.33		807	15	
12.80		280.9	4.8	
14.08		132.0	4.2	
15.33		56.6	1.6	
16.58		28.53	0.54	
17.79		19.51	0.39	
19.06		19.95	0.40	
20.30		23.2	1.0	
21.56		25.07	0.48	
22.82		20.78	0.37	
24.06		16.69	0.53	
25.32		11.84	0.19	
27.81		5.92	0.11	
30.31		2.848	0.097	
32.80		1.412	0.034	
35.30		0.858	0.018	
37.81		0.588	0.017	
40.33		0.438	0.016	
42.83		0.297	0.013	
45.31		0.1942	0.0074	
45.30	0.98	0.198	0.018	179.5
47.82		0.1031	0.0034	
50.31		0.0475	0.0022	
52.81		0.0220	0.0014	
55.31		0.01314	0.00089	
57.81		0.0127	0.0012	
60.31		0.0102 ±	0.0013	

one of the most noticeable features of the present data is the monotonic fall of the cross section with angle, apart from a single oscillation around 20–30°. This discrepancy cannot be ascribed to experimental angular smearing or to contamination from inelastic processes as particular care was taken in the present work to achieve high angular and energy resolution.

The first stage in the optical model analysis of the new data is to try to explain the smooth decrease in the differential cross sections. The data for aluminium were chosen for detailed analysis because it is a fairly light nucleus, so the computing time is not too long, and because a marked discrepancy between the observed and calculated polarizations was found in previous work on this nucleus [6].

A series of calculations was made by varying the parameters U, W, a_1, a_2 and $a_3 = a_4$ in turn, and in each case the marked oscillations persisted. The next variation studied was the effect of different radii for the real and imaginary parts of the potential. Keeping the radius of the real part constant at $r_1 = 1.25$ f (1 f $= 10^{-13}$ cm), the radius of the imaginary part was progressively increased until at $r_2 = 1.75$ f it was found that the cross section fell smoothly from 25° to 55°. The corresponding reaction cross section, however, was too high, but it was found possible to reduce it to the experi-

Table 7. Iron.

Scattering angle θ_{lab} (degrees)	Rms angular resolution $\Delta\,\theta_{lab}$ (degrees)	Differential cross section σ_{lab} (mb/sterad)		Mean proton energy E_{lab} (MeV)
10.34	0.69	889	±22	182.4
12.79		214.1	3.4	
14.14		66.4	1.5	
15.32		29.30	0.91	
15.93		27.73	0.78	
16.31		26.59	0.69	
16.51		27.33	0.71	
17.82		36.36	0.73	
19.01		42.65	0.81	
20.33		44.03	0.42	
21.51		37.53	0.75	
22.83		25.09	0.31	
24.04		18.78	0.43	
25.33		12.30	0.15	
27.80	0.82	4.78	0.12	
30.31		3.113	0.057	
32.81		2.042	0.037	
35.31		1.340	0.026	
37.82		0.887	0.020	
40.31		0.555	0.013	
42.81		0.2959	0.0101	
45.31		0.1427	0.0063	
47.81		0.0601	0.0040	
50.31		0.0417	0.0030	
52.81		0.0331	0.0024	
55.30		0.0207	0.0016	
50.32	1.38	0.0537	0.0040	175.5
55.33		0.0279	0.0019	
60.30		0.01028	0.00097	
65.30		0.00251 ±	0.00043	

mental value by reducing both r_1 and r_2 in the same ratio without losing the qualitative agreement with the differential cross section. Subsequent alteration of the absorbing potential W enabled the oscillation around 23° to be fitted to the experimental data without spoiling the agreement with the measured reaction cross section. A preliminary account of this study of the effects of different radii has already been published [24], together with some of the angular distributions obtained. In all this work the radii r_3 and r_4 of the spin-orbit potentials were kept equal to the corresponding radii r_1 and r_2 of the central potentials.

The primary aim of this work was to fit the differential cross section, but it was found that at the same time the fit to the polarization was substantially improved. In particular, the minimum around 25° is given by the model, whereas previously there was only a slight oscillation in the polarization at this angle. The present data for aluminium may therefore be qualitatively fitted by an optical potential of the form (1) with the imaginary part of the potential extending some 30 % beyond the real part.

A potential of this type was then used to calculate the differential cross sections,

Table 8. Indium.

Scattering angle θ_{lab} (degrees)	Rms angular resolution $\Delta\,\theta_{\text{lab}}$ (degrees)	Differential cross section σ_{lab} (mb/sterad)		Mean proton energy E_{lab} (MeV)
10.31	0.67	599	±10	181.8
12.06		71.9	1.2	
12.81		57.4	1.7	
14.06		123.9	2.1	
15.35		171.1	3.9	
16.54		166.3	3.0	
17.80		125.3	2.1	
20.32		31.13	0.62	
22.08		11.67	0.26	
22.81		9.43	0.31	
24.02		11.74	0.31	
25.29		12.62	0.29	
26.56		11.41	0.27	
27.81		9.82	0.35	
29.06		5.85	0.16	
30.29		3.26	0.13	
32.80		1.792	0.079	
35.31		1.262	0.074	
35.31	1.07	1.353	0.030	182.5
37.81		0.813	0.021	
40.31		0.537	0.016	
42.81		0.283	0.013	
45.31		0.1415	0.0076	
47.81		0.0728	0.0054	
50.30		0.0548	0.0047	
52.81		0.0338	0.0021	
55.31		0.0169	± 0.0025	

polarizations and reaction cross sections for elastic scattering from the other nuclei studied in the present work. In each case overall qualitative agreement was found, with the observed oscillation around 25° followed by a steady decrease of the differential cross section well reproduced by the model.

Further adjustment of the parameters enabled the agreement with the experimental data to be improved for each individual nucleus, and the best fits obtained are shown in Figs. 6–21, and the corresponding parameters in Table 10. As the calculations are rather lengthy (those for gold, for example, had to take into account 35 partial waves) it was possible to make only about 8–10 calculations for each nucleus. The fits shown could therefore certainly be improved if more detailed parameter variations were made. Table 10 also shows the values of Δ, i.e. the measures of the goodness of fit, defined by

$$\Delta = \sum \left(\frac{E - T}{\delta E} \right)^2 ,$$

where T is the theoretical value and $E \pm \delta E$ the experimental, and the summation extends over all the experimental points. The values of Δ obtained are high, but this is most likely more attributable to the incompleteness of the present analysis than

Table 9. Gold.

Scattering angle θ_{lab} (degrees)	Rms angular resolution $\Delta\theta_{\text{lab}}$ (degrees)	Differential cross section σ_{lab} (mb/sterad)		Mean proton energy E_{lab} (MeV)
9.33	0.66	1584	±27	181.8
11.57		400.0	7.6	
14.07		566	10	
10.32	0.77	557	16	181.5
12.81		531	11	
15.31		293.4	5.6	
17.82		59.0	1.3	
19.31		29.96	0.72	
20.33		40.8	1.0	
21.59		51.9	1.2	
22.81		45.8	1.1	
25.31		19.21	0.44	
27.81		6.57	0.22	
29.07		6.55	0.21	
30.34		6.10	0.22	
31.57		5.27	0.18	
32.83		3.84	0.12	
30.32	1.29	5.86	0.10	182.7
35.31		1.952	0.041	
37.81		1.056	0.027	
40.31		0.661	0.020	
42.80		0.412	0.015	
44.05		0.321	0.013	
45.31		0.260	0.012	
47.80		0.1209	0.0079	
50.31		0.0842	± 0.0064	

to any inadequacy of the seven-parameter model. In calculating Δ no allowance was made for the effect of the uncertainty in angle and the angular resolution of the detecting apparatus. If this is included Δ is substantially reduced (cf. Figs 20 and 21 where the effect of the angular resolution is shown). New computer programmes are at present being written, and will be applied to improve the optical model analyses made here.

To illustrate the sensitivity of the distributions to individual variations of the optical model parameters, a series of calculations was made with different values of U, W, U_S, W_S, r_1, r_2 and a for aluminium. These are shown in Figs. 22–35. It is seen that the differential cross sections are mainly affected in the following way: U and U_S displace the curves vertically without altering their shapes, a determines the average slope and the other parameters regulate the diffraction pattern. It is also interesting to note the effects of parameter variations on the polarization. The radial parameters r_1, r_2 and a leave the first polarization maximum essentially unaffected but change the slopes of the polarization oscillations in a characteristic way. The potential depth parameters on the other hand alter the first polarization maximum but leave the oscillations unaffected. The values of the reaction cross sections are also given in Figs. 22–35. As might be expected the reaction cross section is very insensitive to the parameters which determine the real parts of the potential.

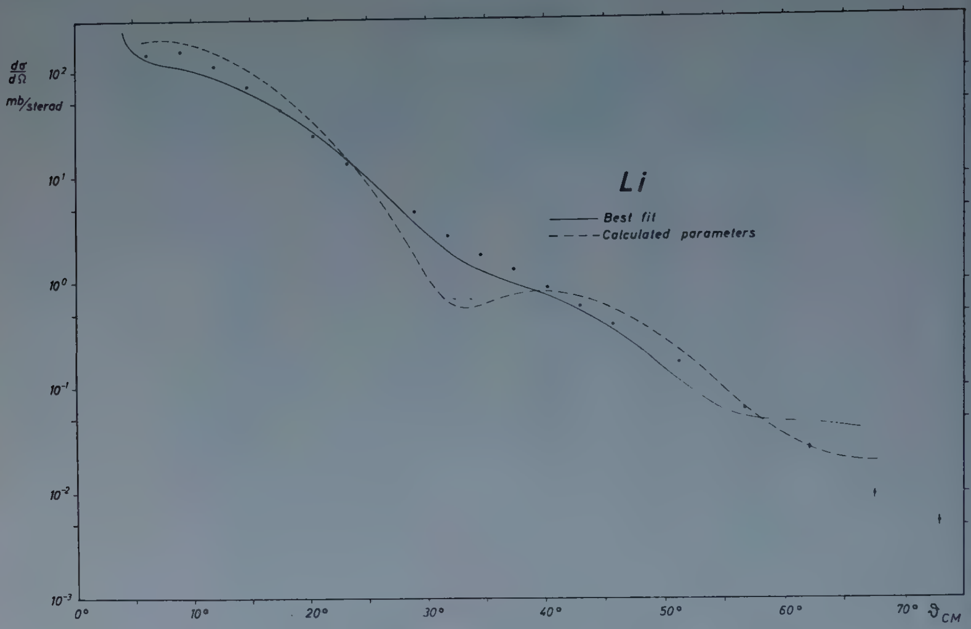

Fig. 6. Differential cross sections in CM system for elastic scattering from lithium. All details about the theoretical curves are given in Tables 10 and 11.

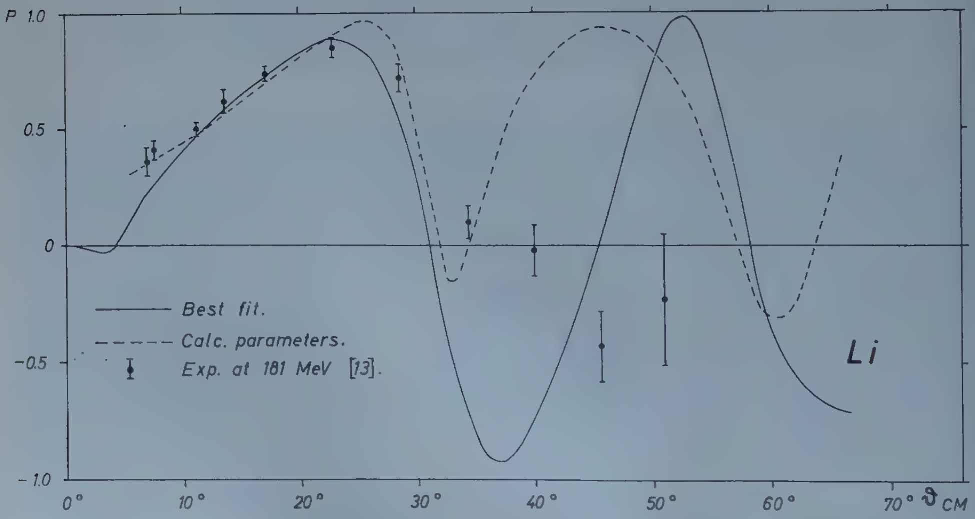

Fig. 7. Polarization of protons elastically scattered from lithium. All details about the theoretical curves are given in Tables 10 and 11. The energy difference between experimental points and theoretical curves has in all polarization diagrams been approximately corrected for by transforming the angular scale for the experimental points in such a way that $\vartheta \sqrt{E}$ was kept constant for each point.

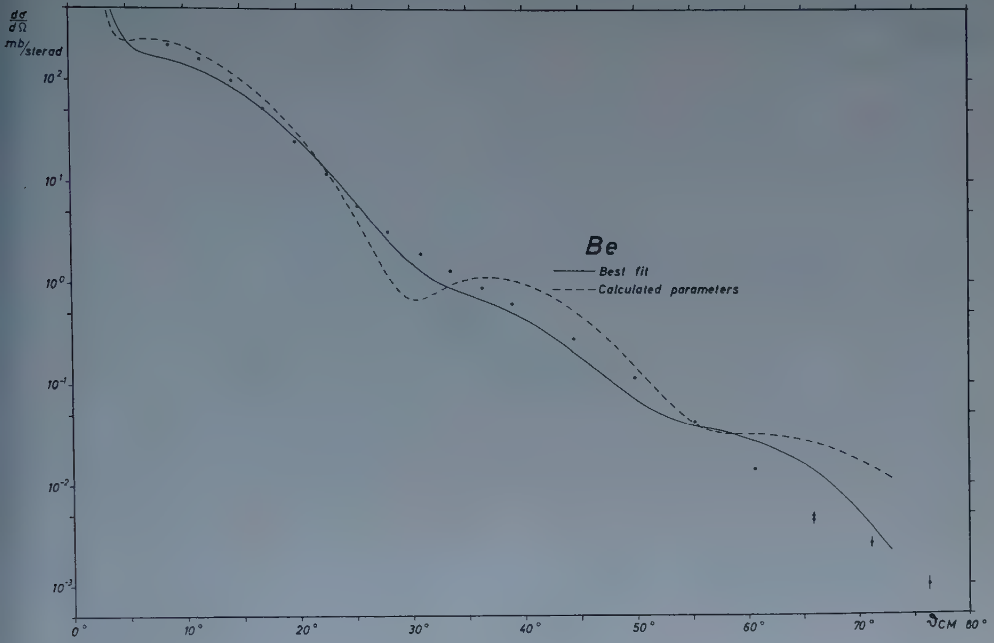

Fig. 8. Differential cross sections in CM system for elastic scattering from beryllium.

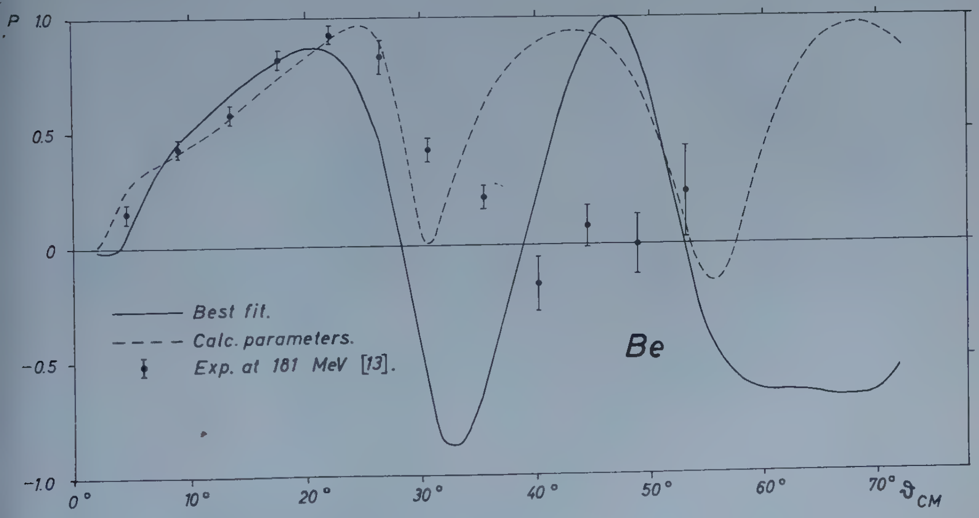

Fig. 9. Polarization of protons elastically scattered from beryllium.

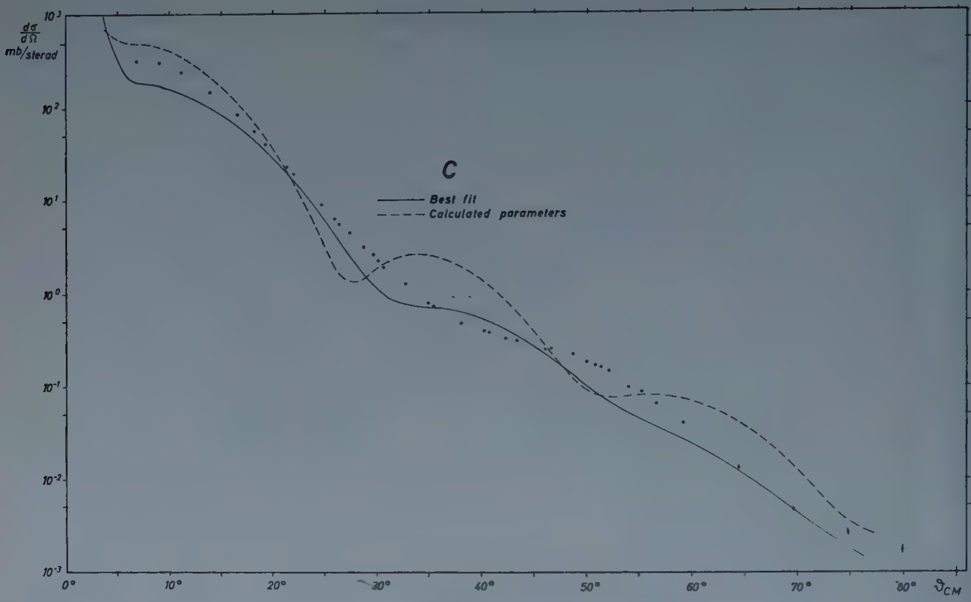

Fig. 10. Differential cross sections in CM system for elastic scattering from carbon.

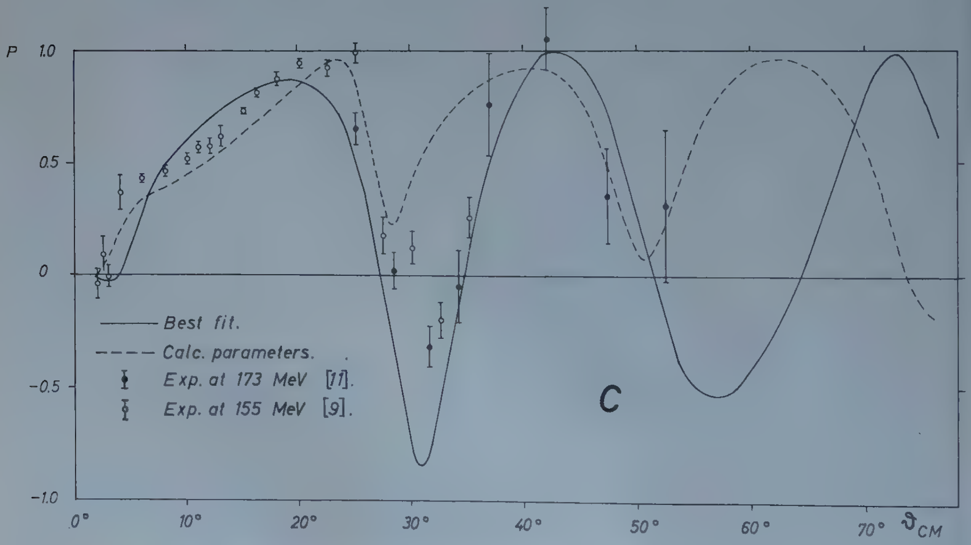

Fig. 11. Polarization of protons elastically scattered from carbon.

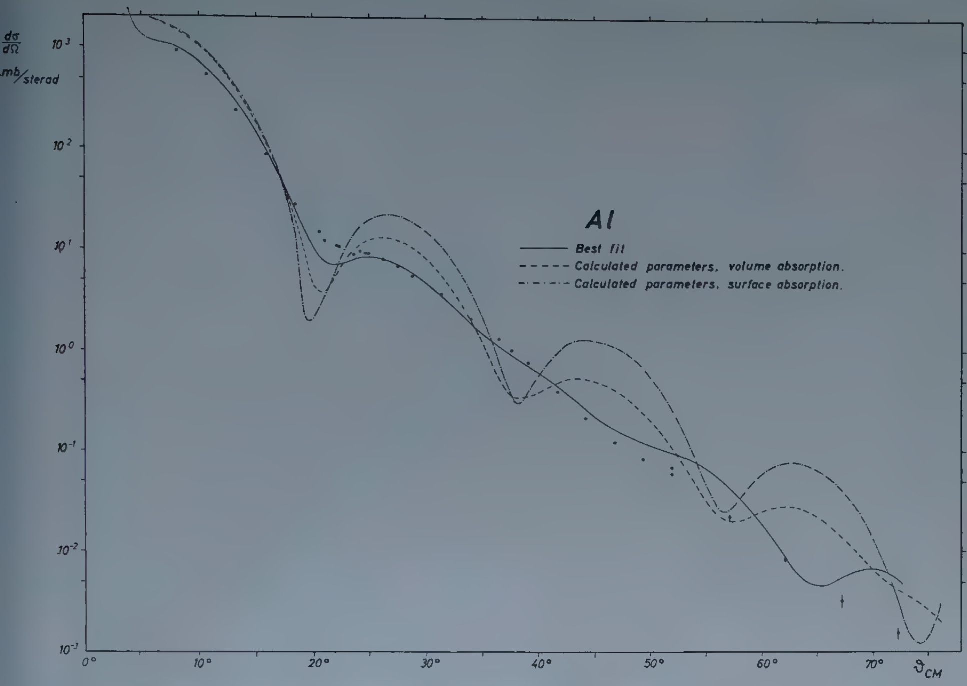

Fig. 12. Differential cross sections in CM system for elastic scattering from aluminium.

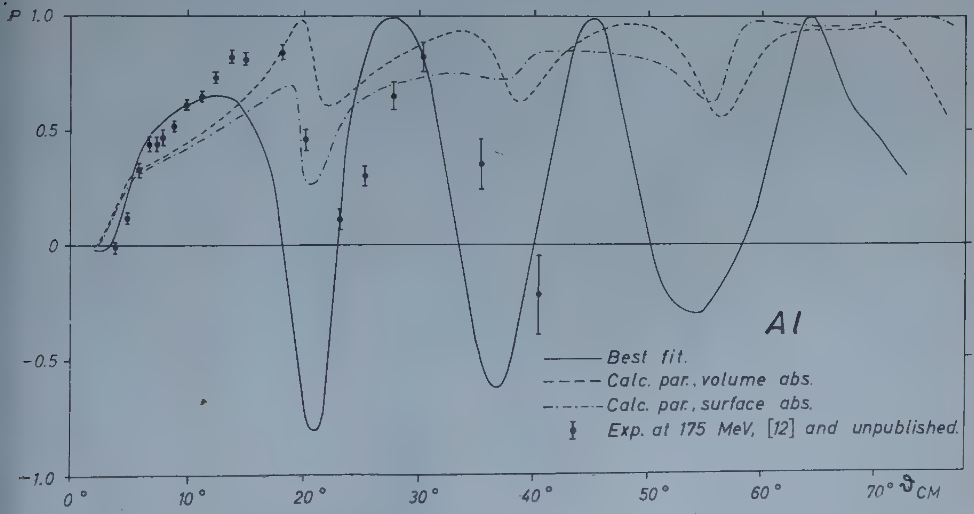

Fig. 13. Polarization of protons elastically scattered from aluminium.

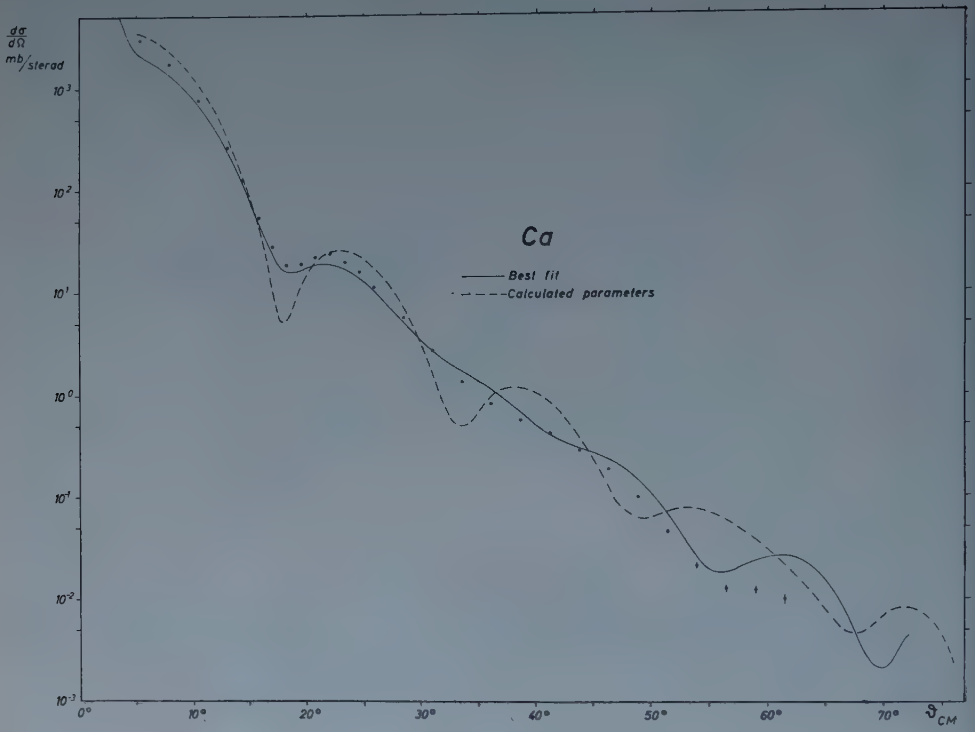

Fig. 14. Differential cross sections in CM system for elastic scattering from calcium.

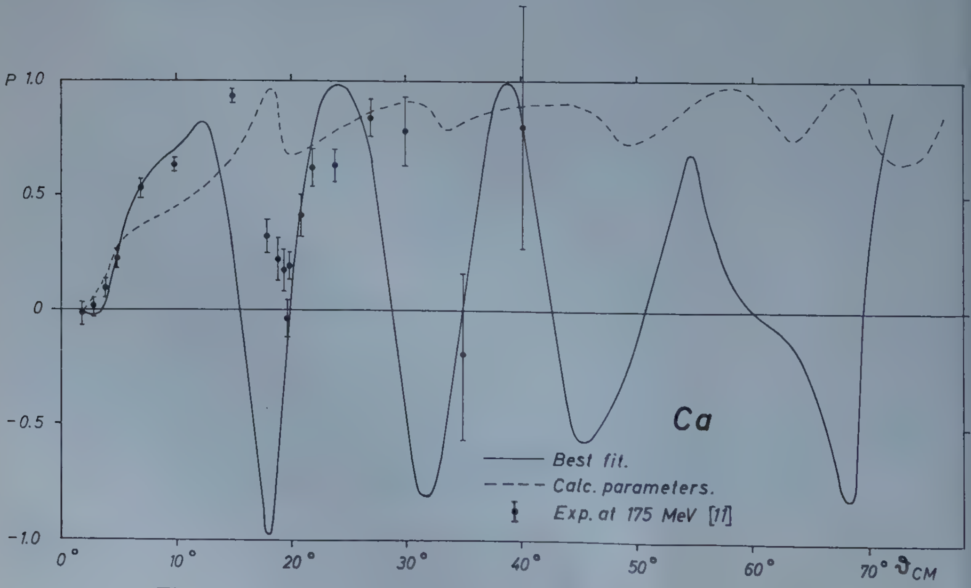

Fig. 15. Polarization of protons elastically scattered from calcium.

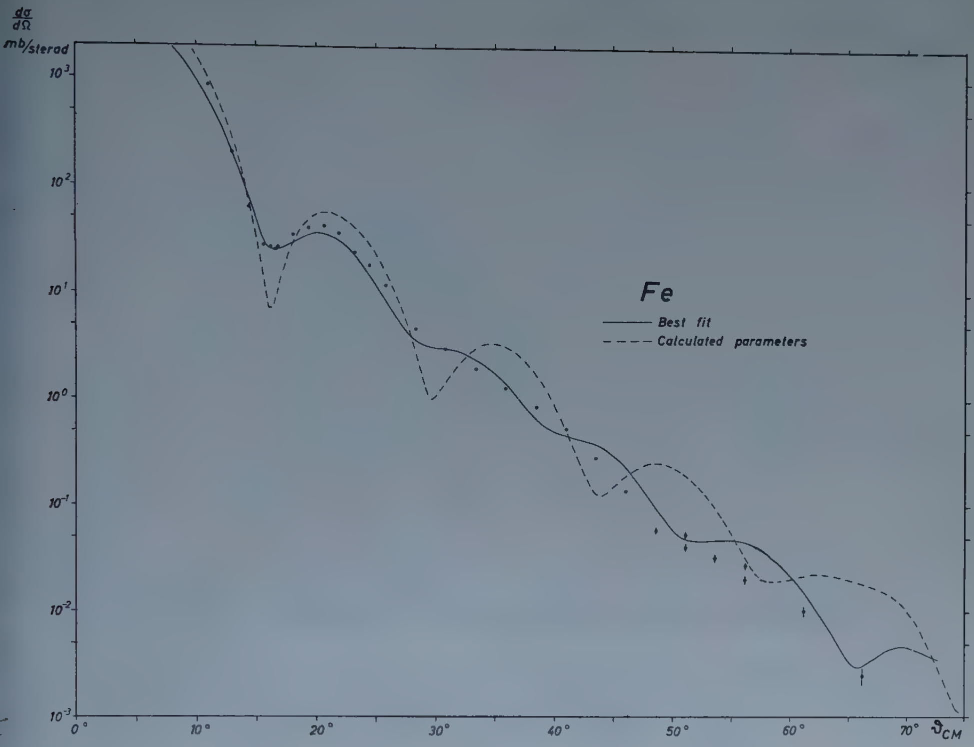

Fig. 16. Differential cross sections in CM system for elastic scattering from iron.

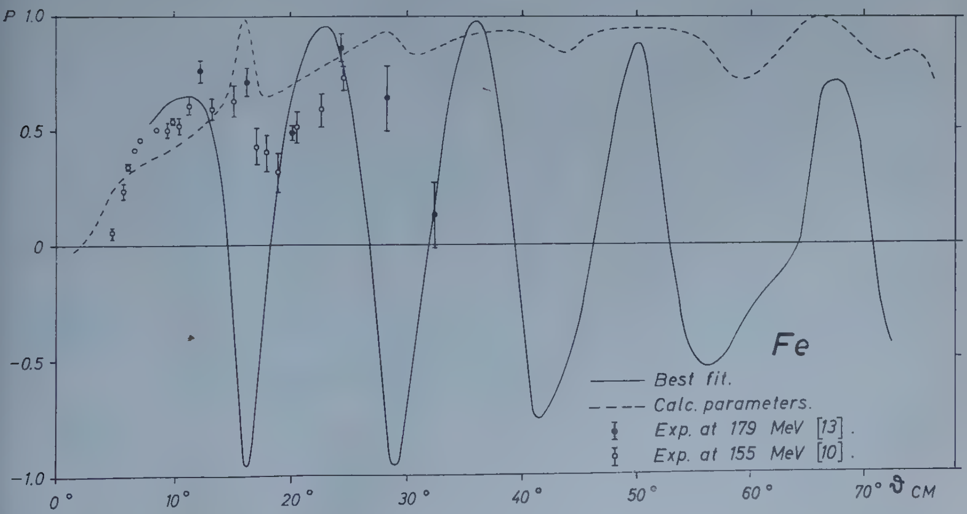

Fig. 17. Polarization of protons elastically scattered from iron.

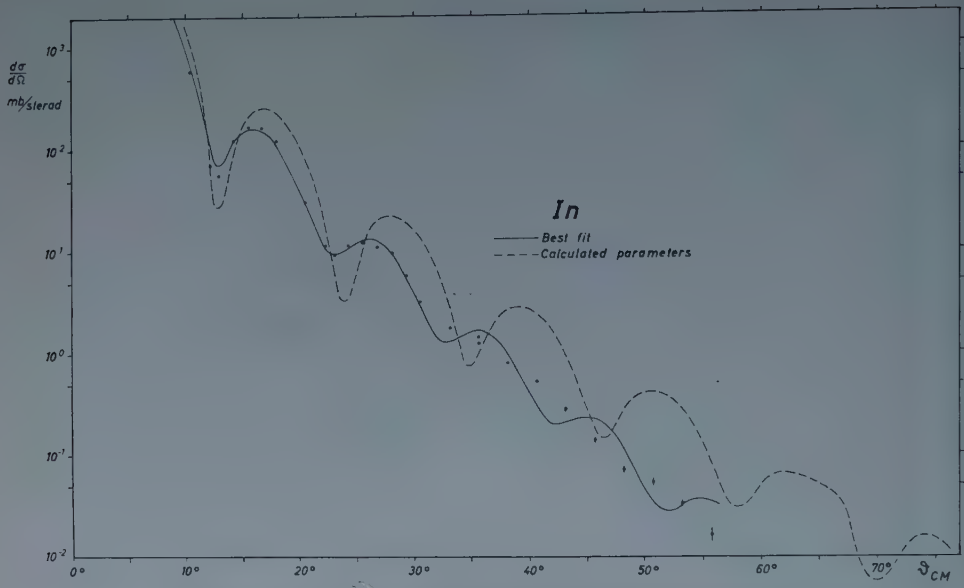

Fig. 18. Differential cross sections in CM system for elastic scattering from indium.

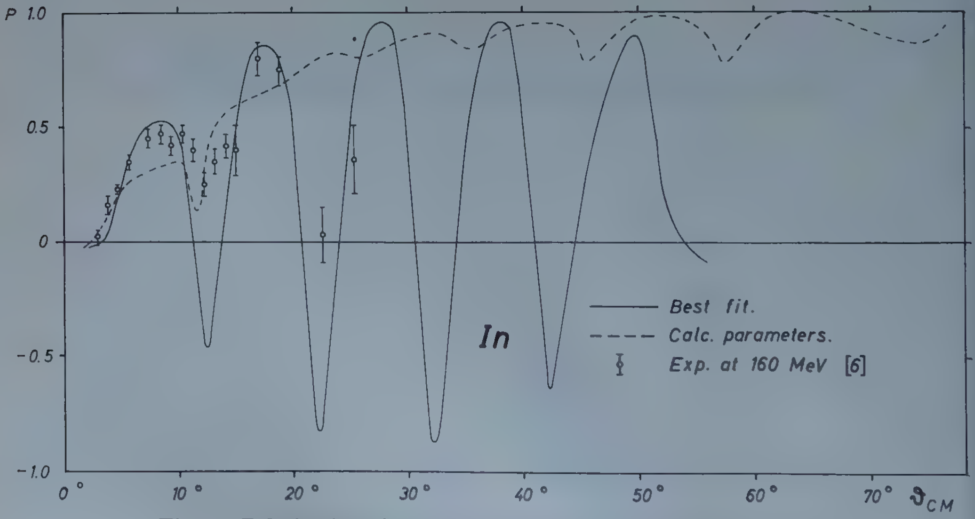

Fig. 19. Polarization of protons elastically scattered from indium.

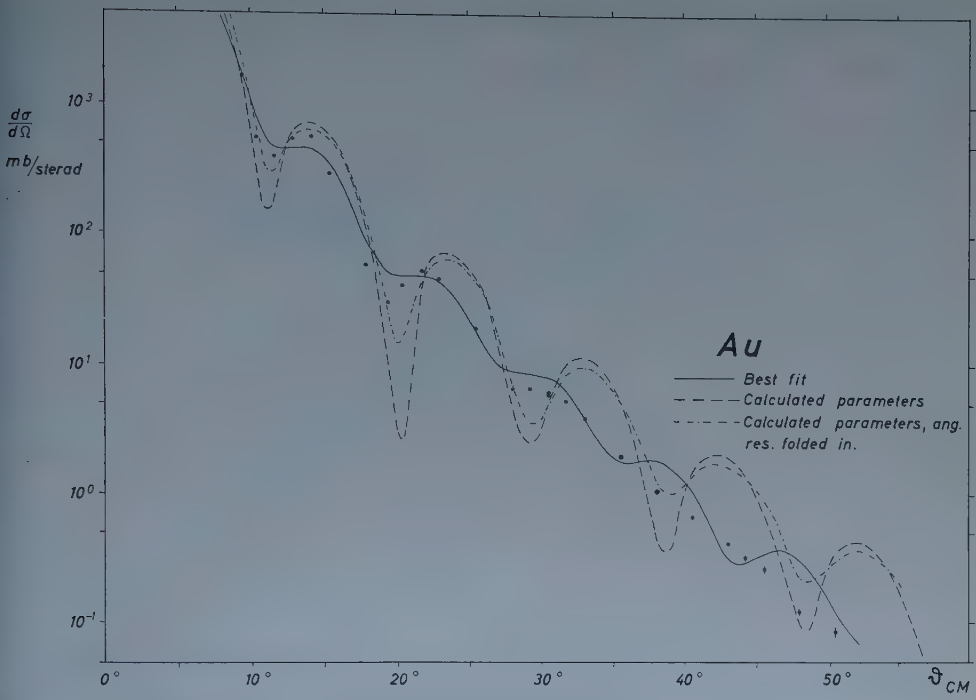

Fig. 20. Differential cross sections in CM system for elastic scattering from gold.

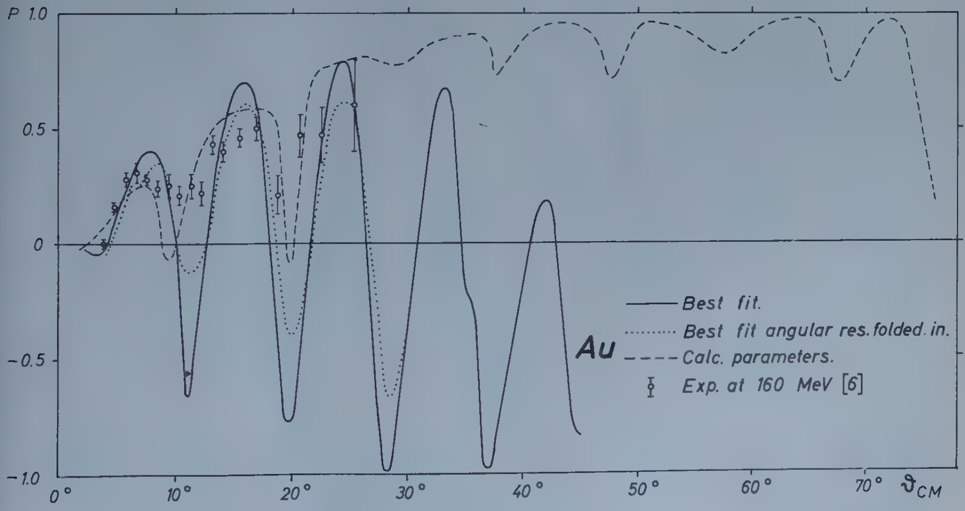

Fig. 21. Polarization of protons elastically scattered from gold.

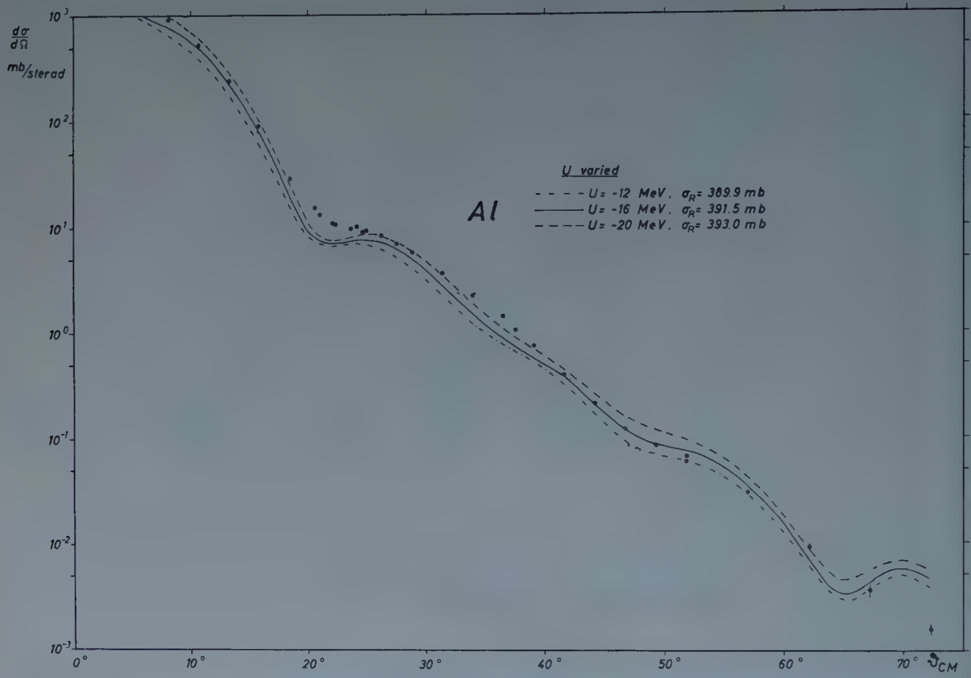

Fig. 22. The effect of varying potential parameters on the differential cross sections for aluminium. The parameters of the solid curve is: $U = -16$ MeV, $W = -8$ MeV, $U_S = 2.5$ MeV, $W_S = -1.0$ MeV, $r_1 = r_3 = 1.15$ f, $r_2 = r_4 = 1.50$ f and $a = a_1 = a_2 = a_3 = a_4 = 0.55$ f.

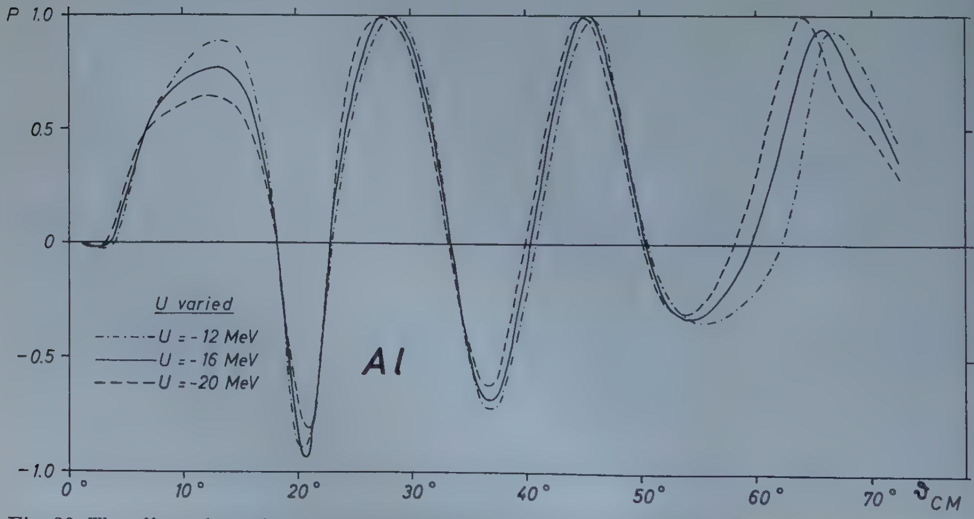

Fig. 23. The effect of varying potential parameters on the polarization for aluminium. Parameters of the solid curve are given in the text to Fig. 22.

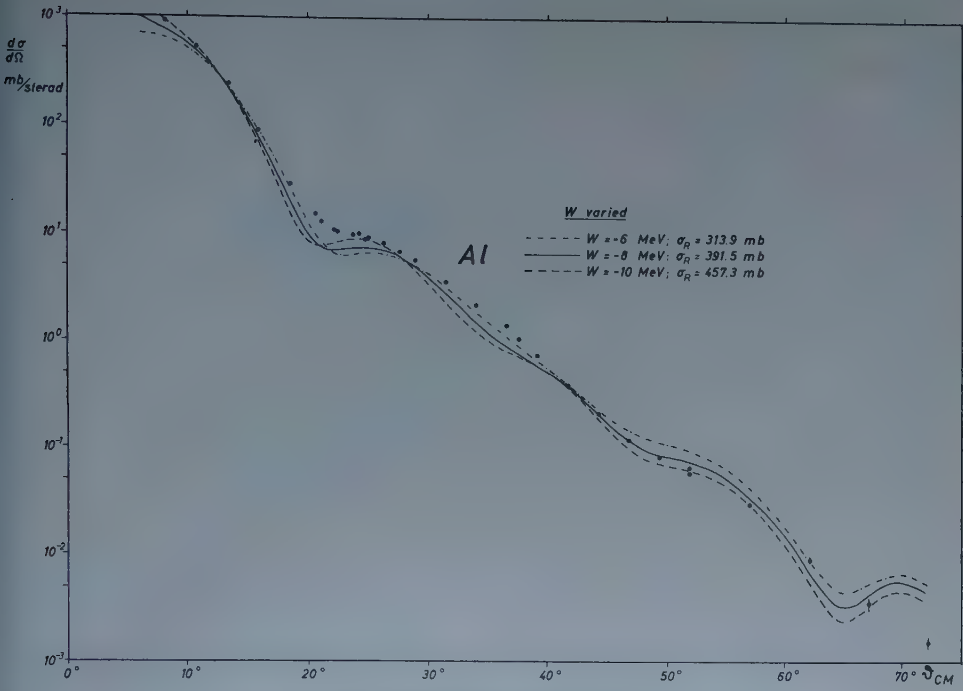

Fig. 24. See text to Fig. 22.

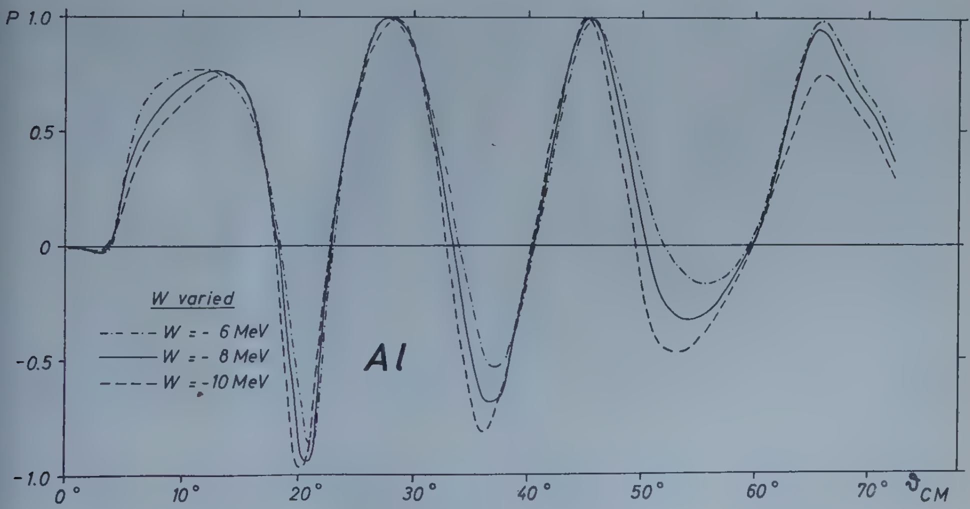

Fig. 25. See text to Fig. 23.

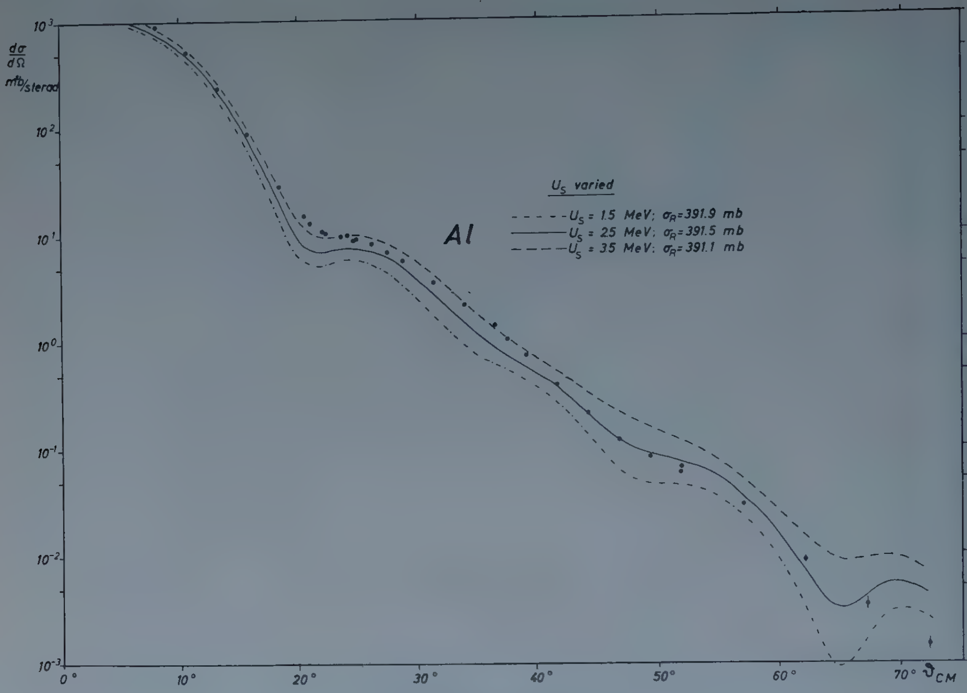

Fig. 26. See text to Fig. 22.

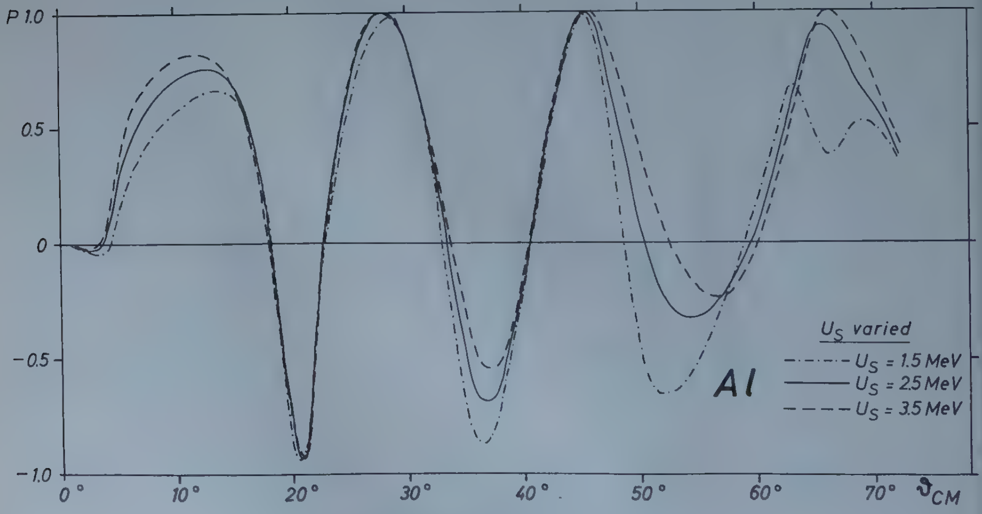

Fig. 27. See text to Fig. 23.

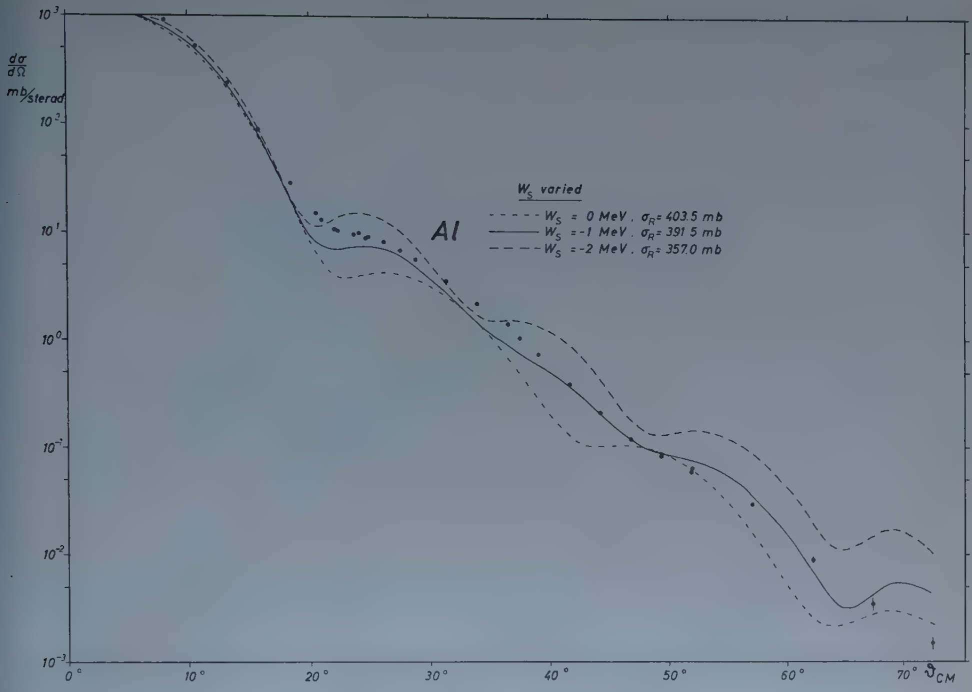

Fig. 28. See text to Fig. 22.

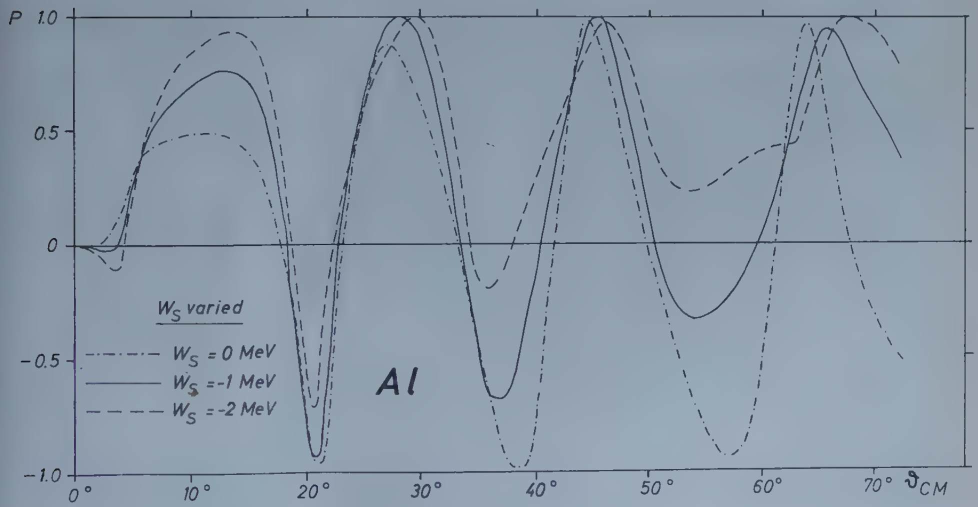

Fig. 29. See text to Fig. 23.

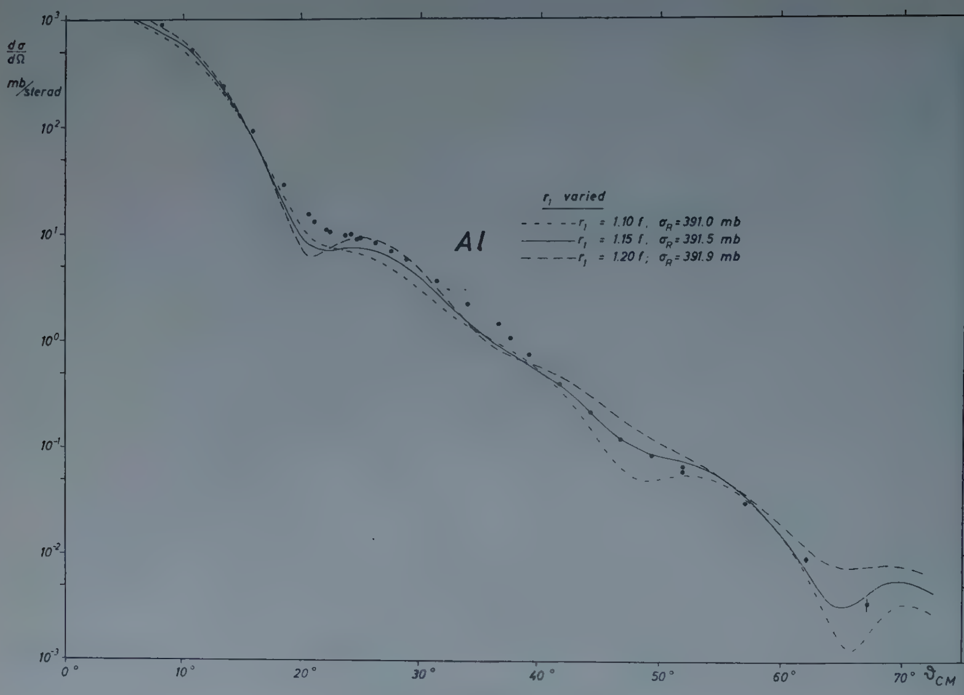

Fig. 30. See text to Fig. 22.

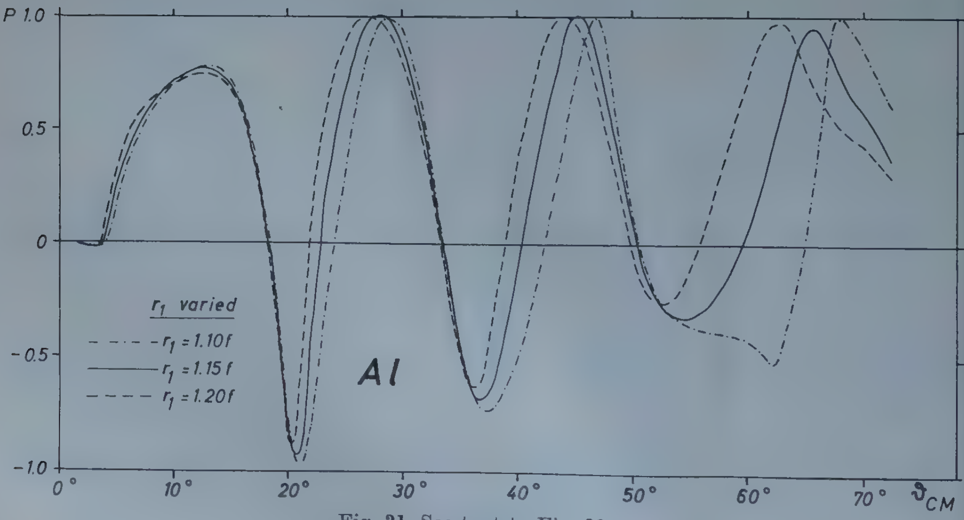

Fig. 31. See text to Fig. 23.

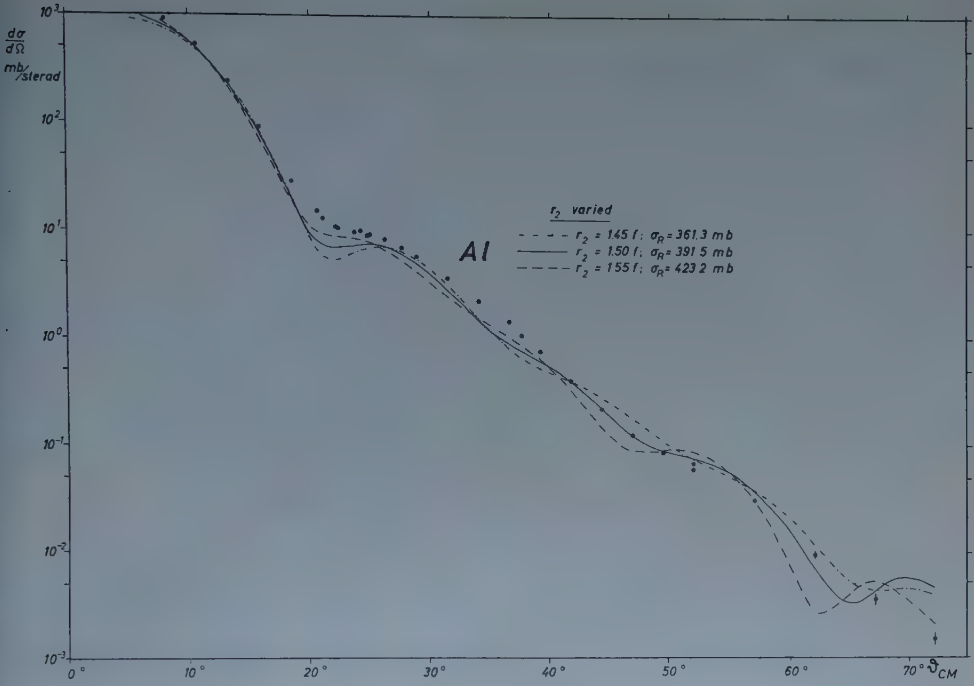

Fig. 32. See text to Fig. 22.

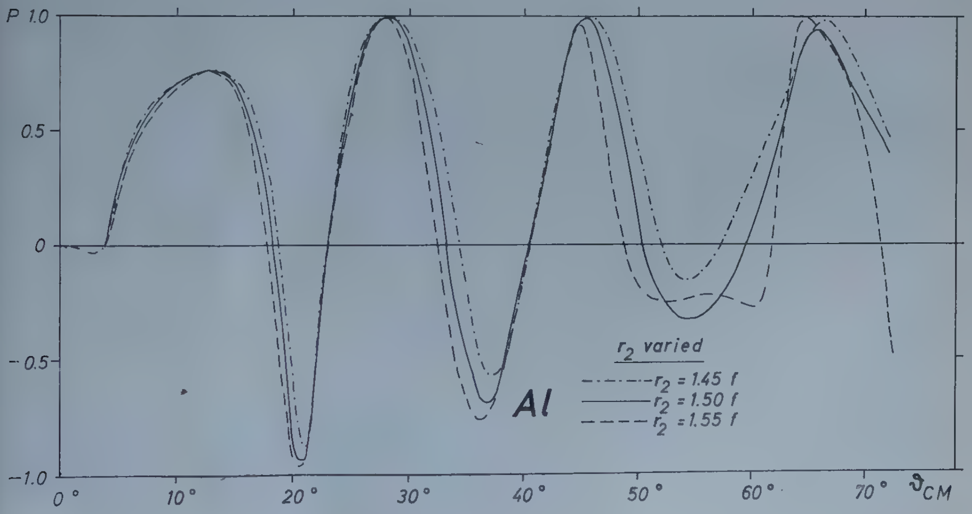

Fig. 33. See text to Fig. 23.

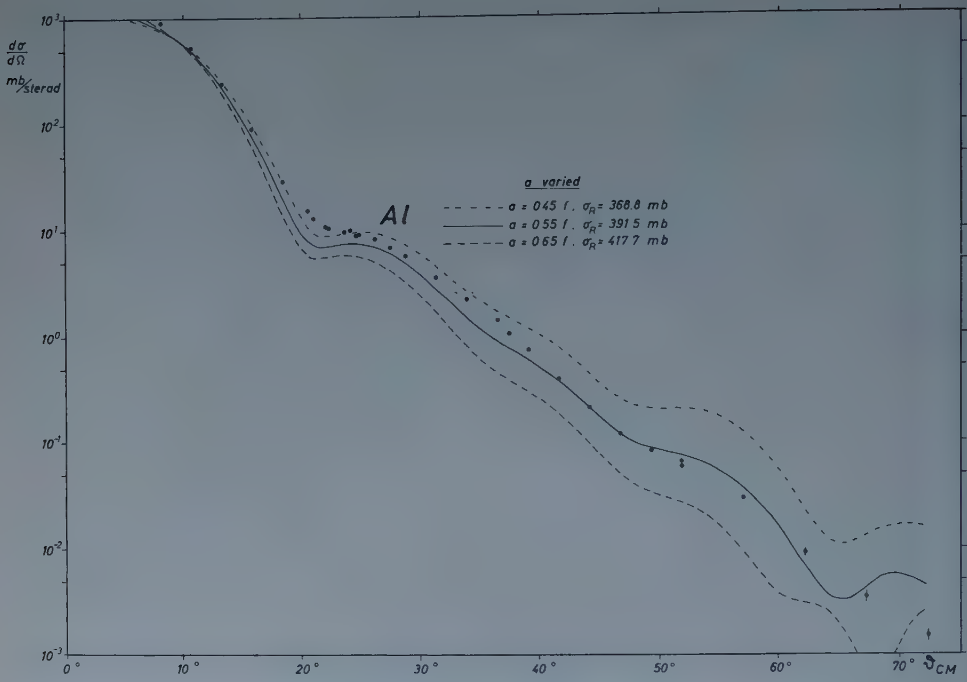

Fig. 34. See text to Fig. 22.

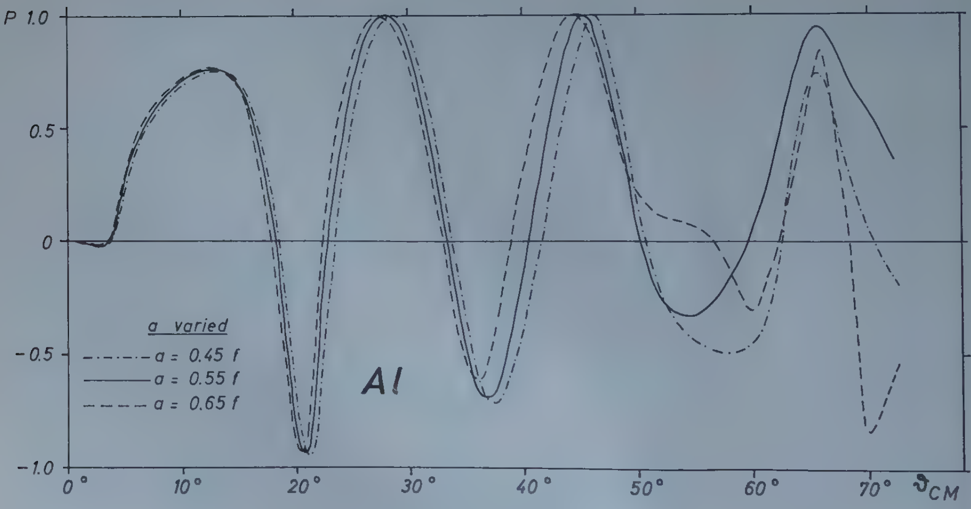

Fig. 35. See text to Fig. 23.

Table 10. Optical model parameters giving the best fit to the experimental results.

The calculated and measured reaction cross sections are compared. The values of Δ_σ and Δ_p that are a measure of the deviation between the calculated and measured differential cross sections and polarizations are also given. N_σ and N_p are the number of experimental measurements of differential cross sections and polarizations respectively. All energies are given in MeV, all lengths in fermis and all cross sections in millibarns.

Nucleus	E_{lab}	$-U$	r_1	$-W$	r_2	U_S	W_S	a	σ_R (Th)	σ_R (Exp)	N_σ	Δ_σ	N_p	Δ_p
Lithium	182.7	16	1.00	10	1.55	2.5	−1	0.4	153	149.0 ± 3.0	19	3392	11	244
Beryllium	182.7	16	1.00	10	1.48	2.5	−1	0.5	186	185.5 ± 4.5	19	4425	12	914
Carbon	183.0	16	1.00	10	1.34	2.5	−1	0.5	183	212.3 ± 4.8	41	11773	20	437
Aluminium	183.0	20	1.15	8	1.50	2.5	−1	0.55	393	390 ± 10	30	3904	20	2270
Calcium	181.5	16	1.18	8	1.51	2.5	−1	0.55	544	524 ± 14	28	2247	19	968
Iron	182.4	16	1.15	10	1.43	2.5	−1	0.55	711	662 ± 19	28	2237	18	770
Indium	181.8	16	1.20	10	1.39	2.5	−1	0.63	1183	1165 ± 34	26	3166	17	731
Gold	181.5	16	1.15	10	1.38	2.5	−1	0.55	1660	1660 ± 50	25	5545	18	618

4.3. *Calculation of potential parameters*

The six-parameter local optical potential was first expressed in terms of the forward amplitudes of the nucleon-nucleon scattering matrix and the nuclear density by Riesenfeld and Watson [25]. It was subsequently shown by Bethe [26] and by McManus and Thaler [27] that the inclusion of the angular dependence of these amplitudes will imply different radii for the potential terms. Extensive studies along these lines have been made by Cromer [28]. In the present parameter calculation the method described in detail by Kerman, McManus and Thaler [7] was followed.

The nucleon-nucleon scattering matrix was assumed to have the usual form

$$M(q) = A(q) + B(q)\,\sigma_{1n}\sigma_{2n} + C(q)\,(\sigma_{1n}+\sigma_{2n}) + E(q)\,\sigma_{1q}\sigma_{2q} + F(q)\,\sigma_{1p}\sigma_{2p}, \tag{2}$$

where $\hbar q$ is the momentum transfer and the amplitudes depend on isotopic spin which will be indicated by indices. For even-even nuclei the B, E and F terms cancel exactly when the spin average over the target nucleons is taken; they were always neglected in the calculations below. The exact number of neutrons and protons in the nuclei was taken into account using the following spin averages for A and C:

$$\overline{A(q)} = \tfrac{1}{4}(A_0 + 3A_1) + \frac{N-2Z}{4N}(A_0 - A_1), \tag{3}$$

$$\overline{C(q)} = \tfrac{1}{4}(C_0 + 3C_1) + \frac{N-2Z}{4N}(C_0 - C_1), \tag{4}$$

where N is the number of nucleons and Z the charge of the target nucleus. Instead of $C(q)$ it is more convenient to use $\hat{C}(q)$ given by

$$\hat{C}(q)\cdot k\sin\theta = k_0 C(q), \tag{5}$$

where $\theta =$ the scattering angle in the many-body CM system,
$\hbar k =$ the momentum of the incident proton in the many-body CM system,
$\hbar k_0 =$ the momentum of the incident proton in the two-body CM system.

If the optical potential (1) is written

$$V(r) = \frac{N-1}{N} \cdot V_{\mathrm{Coul}}(r) + V_c(r) + \frac{1}{r} \cdot \frac{d}{dr} V_{so}(r)\, \boldsymbol{l} \cdot \boldsymbol{\sigma}. \tag{6}$$

Kerman *et al.* [7] obtain

$$V_c(r) = -\frac{2\hbar^2}{m} \cdot \frac{N-1}{(2\pi)^2} \cdot \int e^{-i\boldsymbol{q}\cdot\boldsymbol{r}} \cdot F(q)\, \overline{A(q)}\, d\boldsymbol{q}, \tag{7}$$

$$V_{so}(r) = -\frac{2i\hbar^2}{m} \cdot \frac{N-1}{(2\pi)^2} \int e^{-i\boldsymbol{q}\cdot\boldsymbol{r}} \cdot \frac{\overline{\hat{C}(q)}}{k_0 k}\, d\boldsymbol{q}, \tag{8}$$

where m is the nucleon mass and $F(q)$ the nuclear form factor. If the nuclear density is denoted by $\varrho(r)$, normalized so that $\int \varrho(r)\, d\boldsymbol{r} = 1$, the nuclear form factor is given by

$$F(q) = \int e^{i\boldsymbol{q}\cdot\boldsymbol{r}} \varrho(r)\, d\boldsymbol{r}. \tag{9}$$

The differential cross sections obtained after solving the Schrödinger equation using the potential (6) are to be multiplied by $(N/[N-1])^2$ before being compared with experiment. The calculation of the potential parameters is illustrated below for the real central term. (The other parameters were obtained in a corresponding manner.) There are three parameters to be determined: U, R_1 and a_1. The following equations are valid to a very good approximation:

$$\int U f_1(r)\, d\boldsymbol{r} = \frac{4\pi}{3} R_1 (R_1^2 + \pi^2 a_1^2) \cdot U, \tag{10}$$

$$\int U f_1(r)\, r^2\, d\boldsymbol{r} = \left(\tfrac{3}{5} R_1^2 + \tfrac{7}{5} \pi^2 a_1^2\right) \cdot \int U f_1(r)\, d\boldsymbol{r}, \tag{11}$$

$$\int U f_1(r)\, r^4\, d\boldsymbol{r} = \left(\tfrac{3}{7} R_1^4 + \tfrac{18}{7} R_1^2 \cdot \pi^2 a_1^2 + \tfrac{31}{7} \pi^4 a_1^4\right) \cdot \int U f_1(r)\, d\boldsymbol{r}. \tag{12}$$

Integration of the real part of equation (7) gives

$$\int \mathrm{Re}\{V_c(r)\}\, d\boldsymbol{r} = -4\pi \cdot \frac{\hbar^2}{m} (N-1)\, \mathrm{Re}\{\overline{A(0)}\}, \tag{13}$$

$$\int \mathrm{Re}\{V_c(r)\}\, r^2\, d\boldsymbol{r} = \left[-3 \frac{F''(0)}{F(0)} - 3 \frac{\mathrm{Re}\{\overline{A''(0)}\}}{\mathrm{Re}\{\overline{A(0)}\}}\right] \cdot \int \mathrm{Re}\{V_c(r)\}\, d\boldsymbol{r}, \tag{14}$$

$$\begin{aligned} \int \mathrm{Re}\{V_c(r)\}\, r^4\, d\boldsymbol{r} = \Bigg[& 5 \cdot \frac{F^{\mathrm{IV}}(0)}{F(0)} + 30 \frac{F''(0)}{F(0)} \cdot \frac{\mathrm{Re}\{\overline{A''(0)}\}}{\mathrm{Re}\{\overline{A(0)}\}} + \\ & + 5 \frac{\mathrm{Re}\{\overline{A^{\mathrm{IV}}(0)}\}}{\mathrm{Re}\{\overline{A(0)}\}} \Bigg] \cdot \int \mathrm{Re}\{V_c(r)\}\, d\boldsymbol{r}. \end{aligned} \tag{15}$$

Setting (10) = (13), (11) = (14), and (12) = (15) gives three equations from which U, R_1 and a_1 can be determined if $F(q)$ and $A(q)$ are known in a series expansion about $q = 0$ up to terms of the fourth power. From equation (9) $F(0) = 1$, and the deriva-

Table 11. Calculated optical potential parameters.

All lengths are given in fermis and all energies in MeV.

	Li	Be	C	Al volume absorption	Al surface absorption	Ca	Fe	In	Au
r_1	1.609	1.509	1.418	1.241	1.241	1.202	1.163	1.115	1.109
a_1	0.465	0.485	0.509	0.618	0.618	0.688	0.690	0.710	0.746
U	− 8.45	−10.39	−12.88	−19.44	−19.44	−21.55	−24.63	−29.51	−31.03
r_2	1.475	1.390	1.310	1.184	0.994	1.153	1.134	1.103	1.103
a_2	0.450	0.471	0.496	0.597	0.949	0.665	0.662	0.673	0.704
W	−10.44	−12.52	−14.82	−20.91	−23.66	−22.16	−25.33	−30.01	−31.39
α	1.000	1.000	1.000	1.000	0.198	1.000	1.000	1.000	1.000
r_2'					0.946				
b					1.135				
r_3	1.299	1.245	1.198	1.125	1.125	1.120	1.105	1.091	1.098
a_3	0.437	0.454	0.477	0.570	0.570	0.637	0.627	0.624	0.647
U_S	1.98	2.33	2.50	3.02	3.02	3.05	3.34	3.70	3.73
r_4	1.306	1.252	1.205	1.130	1.130	1.125	1.108	1.092	1.098
a_4	0.466	0.482	0.503	0.591	0.591	0.655	0.647	0.647	0.670
W_S	− 0.54	− 0.60	− 0.61	− 0.77	− 0.77	− 0.76	− 0.89	− 1.05	− 1.10

tives of $F(q)$ are closely related to the second and the fourth moments of the nuclear density. These moments were found from electron scattering experiments [14]. Interpolation was used for nuclei for which no electron data are available. The values for $A(q)$ were obtained from the Gammel-Thaler nucleon-nucleon potentials by interpolating to 180 MeV between the values tabulated by Kerman *et al.* [7]. The parameters obtained in this manner are given in Table 11. They have been used to calculate the differential cross sections and the polarizations, which are shown in Figs. 6–21 together with the best fits from the phenomenological parameter search. In the case of aluminium two kinds of absorbing potentials were used, one with a pure Saxon–Woods form factor and the other with such a combination of volume and surface absorption that the volume and the second and fourth moments of the potential were still given by equations (13)–(15); i.e. judged by the method used for deriving potentials there should be no difference between the two types of imaginary potentials.

4.4. *Discussion*

The overall agreement between experimental results and the best fits of the phenomenological potential suggests that the optical model is applicable to the large-angle scattering of high-energy protons by nuclei, but this agreement can only be obtained if the radii of the potential terms are allowed to be different. It is seen from Table 10 that $r_2 \approx 1.5\, r_1$ for the lightest nuclei and $r_2 \approx 1.2\, r_1$ for the heavier ones. This conclusion may be modified when more data are available or when more extensive parameter searches are carried out. In particular, when r_3 and r_4 are allowed to differ from r_1 and r_2 respectively, one might find best fits with parameters that are substantially different from those given in Table 10. Such investigations will, however, have to await the completion of faster computer programmes.

The scattering predicted from the potentials with calculated parameters also shows an overall agreement with experimental data. However, the oscillations in the differential cross sections are seen to be too pronounced, indicating that the radial differences may be too small. The polarization patterns are almost free from minima which probably also could be remedied by increasing the radial differences. Now, one should not expect a perfect fit from this derived potential for several reasons. The Gammel-Thaler nucleon-nucleon scattering matrix does not fit nucleon-nucleon data extremely well, the electron scattering data are somewhat uncertain, particularly when interpolations have to be made, terms of $F(q)$ and $M(q)$ in q^6 and higher orders may be effective in determining the form factors (cf. the two Al-curves in Figs. 12 and 13) and the local approximation is uncertain for large angles, in particular in the vicinity of diffraction minima. The effect of a non-local potential at scattering energies up to 25 MeV has been investigated by Wyatt, Wills and Green [29]. They find that nonlocality tends to accentuate rather than wash out diffraction patterns. If this holds also at 180 MeV, the absence of pronounced diffraction minima in the present experiments cannot be explained by the fact that a realistic optical potential should be nonlocal and thus it does not necessarily imply that the local approximation is invalid. The reaction cross sections given by the potentials of Table 11 are compared to experimental data in the preceding paper [8]. From this comparison one may conclude that the magnitude of the imaginary potential W should be reduced by about 20 % for a reasonable agreement between theoretical and experimental reaction cross sections. Such a change would also tend to improve the fits to the differential cross sections at small angles. Generally it would be interesting to see if slight deviations of the potential parameters from the values given in Table 11 are able to produce an optical potential that predicts a scattering which more closely agrees with experimental results.

ACKNOWLEDGEMENTS

We want to thank Professor The Svedberg for his interest and support, Mr. P. Isacsson for the design of the fast electronic circuits, and Mr. Å Svanheden and the cyclotron crew for valuable help during runs. The experimental part of this work was supported by the Swedish Atomic Research Council.

We are grateful to the Director of the Computing Laboratory, Oxford, for the use of the computer, Dr. B. Buck and Mr. R. N. Maddison for their work on the computer programme, and the technical staff for their assistance. Thanks are also due to Dr. K. Parker for performing some preliminary calculations on the A.W.R.E. IBM 709 computer at Aldermaston.

The Gustaf Werner Institute for Nuclear Chemistry, University of Uppsala, Sweden, and the Clarendon Laboratory, Oxford, England.

REFERENCES

1. Taylor, A. E., Reports on Progress in Physics, Vol. XX, p. 86, 1957.
2. Faissner, H., Ergebnisse der exakten Naturwissenschaften, Vol. 32, p. 180, 1959.
3. Squires, E. J., Progress in Nuclear Physics, Vol. 8, p. 47, 1960.
4. Bjorklund, D. F., Blandford, I., and Fernbach, S., Phys. Rev. *108*, 795 (1957).
5. Wilson, R., Phys. Rev. *114*, 260 (1959).
6. Johansson, A., Tibell, G., Parker, K., and Hodgson, P. E., Nucl. Phys. *21*, 383 (1960).
7. Kerman, A. K., McManus, H., and Thaler, R. M., Ann. Phys. *8*, 551 (1959).
8. Johansson, A., Svanberg, U., and Sundberg, O., Arkiv Fysik *19*, 527 (1961).
9. Alphonce, R., Johansson, A., and Tibell, G., Nucl. Phys. *4*, 672 (1957).
10. Alphonce, R., Johansson, A., and Tibell, G., Nucl. Phys. *4*, 643 (1957).

11. Hillman, P., Johansson, A., and Tyrén, H., Nucl. Phys. *4*, 648 (1957).
12. Hillman, P., Johansson, A., and Tibell, G., Phys. Rev. *110*, 1218 (1958).
13. Johansson, A., Tibell, G., and Hillman, P., Nucl. Phys. *11*, 540 (1959).
14. Hofstadter, R., Ann. Rev. Nucl. Sci. *7*, 231 (1957).
15. Tyrén, H., and Maris, Th. A. J., Arkiv Fysik *13*, 609 (1958).
16. Hess, W. N., Rev. Mod. Phys. *30*, 368 (1958).
17. Palmieri, J. N., Cormack, A. M., Ramsey, N. F., and Wilson, R. Ann. Phys. *5*, 299 (1958).
18. Taylor, A. E., Wood, E., and Bird, L., Nucl. Phys. *16*, 320 (1960).
19. Caverzasio, C., and Michalowicz, A., J. phys. radium *21*, 314 (1960).
20. Buck, B., Maddison, R. N., and Hodgson, P. E., Phil. Mag. *5*, 1181 (1960).
21. Bjorklund, D. F., and Fernbach, S., UCRL 5028 (1958), unpublished.
22. Hafner, E. M., Phys. Rev. *111*, 297 (1958).
23. Jastrow, R., and Harris, I., Nucl. Phys. *9*, 437 (1958–59).
24. Hodgson, P. E., Phys. Rev. Letters (1961), in press.
25. Riesenfeld, W. B., and Watson, K. M., Phys. Rev. *102*, 1157 (1956).
26. Bethe, H. A., Ann. Phys. *3*, 190 (1958).
27. McManus, H. M., and Thaler, R. M., Phys. Rev. *110*, 590 (1958).
28. Cromer, A. H., Phys. Rev. *113*, 1607 (1959); and Cornell University thesis (1960), unpublished.
29. Wyatt, P. J., Wills, J. G., and Green, A. E. S., Phys. Rev. *119*, 1031 (1960).

Tryckt den 26 april 1961

Uppsala 1961. Almqvist & Wiksells Boktryckeri AB